Contents lists available at ScienceDirect

Radiation Measurements

journal homepage: www.elsevier.com/locate/radmeas

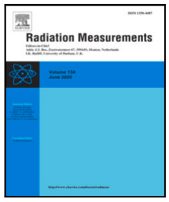

Highlights

Effect of radiation physics on inherent statistics of glow curves from small samples or low doses

Radiation Measurements xxx (xxxx) xxx

John L. Lawless*, R. Chen, V. Pagonis

- Thermoluminescence (TL) is inherently noisy, especially for small samples or low doses.
- The Master Equation predicts how TL noise changes with type of radiation source.
- The theory applies to high-energy radiation sources such as beta, alpha, & gamma.
- Analytical predictions are made of noise as a function of sample shape & orientation.
- Predictions are made for standard deviation, dispersion, skewness, & kurtosis.

Contents lists available at ScienceDirect

Radiation Measurements

journal homepage: www.elsevier.com/locate/radmeas

Effect of radiation physics on inherent statistics of glow curves from small samples or low doses

John L. Lawless [a,*], R. Chen [b], V. Pagonis [c]

[a] Redwood Scientific, Pacifica, CA, USA
[b] Raymond and Beverly Sackler School of Physics and Astronomy, Tel Aviv University, Tel Aviv 69978, Israel
[c] Physics Department, McDaniel College, Westminster, MD 21157, USA

ARTICLE INFO

Keywords:
Luminescence
Radiation effects
Dosimetry
Thermoluminescence
Optically-stimulated luminescence
Single Grain

ABSTRACT

A theory is developed to predict statistical noise in the trap populations of small samples or single grains subjected to high-energy ionizing irradiation. Using a model of the radiation process and a one-trap one-center model of a thermoluminescent (TL) material, the statistical behavior of the number of occupied traps during irradiation is predicted. The model focuses on the inherent physics of the process. Experimental sources of error are not considered. The interaction of radiation with the TL material is modeled in a simple way using the Bethe equation. The trap and center populations in the TL material are modeled both with the conventional phenomenological equations and also the more general Master Equation approach. The theory predicts, as the irradiation process proceeds, the mean, standard deviation, dispersion, skewness, and kurtosis of the probability distribution of occupied traps in the TL material. For the same applied dose, the standard deviation and dispersion of the trap population depend strongly on the type of radiation as well as the shape and orientation of the material. High-energy radiation sources, such as alpha, beta, or gamma rays, are found to produce standard deviations and dispersion much larger than low-energy sources, such UV radiation. The results are summarized in tables which enable, for useful limiting cases, easy calculation of not just standard deviation but also skewness and kurtosis for various radiation sources and geometries.

1. Introduction

The recent publications on single-grain experiments have demonstrated the importance of statistical noise in the thermoluminescence and optically stimulated luminescence processes. Noise can be an issue whenever low doses or small samples are of interest. We will investigate the noise associated with inherent statistical nature of the physical thermoluminescence process of irradiation by energetic particles, such as alpha, beta, and gamma rays. Instrumentation and other experimental sources of noise are not considered. The trap and center populations in the material will be modeled using the master equation approach. To quantify the effect, the irradiation process will be modeled with a simplified Bethe theory. The model will be applied to samples or grains of different shapes to show the importance of both sample shape and orientation for thermoluminescence statistics.

Thermoluminescence, optically stimulated luminescence, and related phenomena have been studied extensively with the first successful models of thermoluminescence emission having appeared over seventy years ago (Randall and Wilkins, 1945a,b; Garlick and Gibson, 1948). When an insulator or semiconductor is irradiated, electrons and/or holes can be excited and subsequently caught in metastable traps. If the material is later heated, typically in an oven, the electrons are released from the traps and some of them will radiatively recombine. Light emitted in this way is called thermoluminescence. These phenomena have found widespread application for dating in archeology and geology as well as for dosimetry. Several books review the theory and applications (Aitken, 1985; McKeever, 1985; Chen and McKeever, 1997; Yukihara and McKeever, 2011; Chen and Pagonis, 2011).

Experimental techniques have been developed for reducing noise or improving the signal-to-noise ratio for thermoluminescence or optically stimulated luminescence measurements of low doses or small samples. One approach for improving the signal-to-noise ratio of thermoluminescence at low doses is rapid heating such as with a CO_2 laser (Gasiot et al., 1982; Bräunlich, 1990; Lawless et al., 2002). For small samples, noise levels can be important even at high doses. For example, specialized instruments have been developed to minimize instrumental noise when measuring luminescence from single-grains (Duller et al., 1999; Bøtter-Jensen et al., 2000; Duller, 2004; Jacobs et al., 2006; Jacobs and Roberts, 2007).

* Corresponding author.
E-mail address: lawless@alumni.princeton.edu (J.L. Lawless).

https://doi.org/10.1016/j.radmeas.2021.106698
Received 30 June 2021; Received in revised form 27 October 2021; Accepted 13 December 2021

To quantify the inherent – as opposed to instrumental – noise of the thermoluminescence process, we will develop a master equation for the trap and center populations during irradiation (van Kampen, 1992; Lawless et al., 2020). Master equations have been used in a wide variety of fields ranging from the analysis of energy distributions of free electrons in both plasmas and solids (Fokker, 1914; Planck, 1917; Dendy, 1990; Kolobov, 2003) to the prediction of the carbon-monoxide vibrational laser (Rich and Treanor, 1970) to general theories of reaction rate constants (Fain, 1981). In the field of thermoluminescence, the master equation approach has been previously used to predict autocorrelation of fluctuations in thermoluminescence intensity (Swandic, 1992, 1996).

We have previously used a master equation to study irradiation from low-energy sources such as ultraviolet light (Lawless et al., 2020). One photon of UV light may produce only one electron–hole pair. In this paper, we investigate the statistical behavior of high-energy radiation sources such as alpha, beta, or gamma rays. For these sources, a single ray may produce thousands or more electron–hole pairs and this can lead to a strong increase in the inherent noise level. When looked at in detail, the physics of irradiation by high-energy particles can be quite complex (National Academy of Sciences, 1964; Salvat et al., 2007; Nuclear Energy Agency, 2019). To illustrate our master equation theory, we will use the Bethe theory for stopping power combined with some simplifying assumptions.

The present theory is focused on the statistical properties of the noise in glow curves or OSL rather than the mean values. Guérin et al. (2015) use a numerical Monte-Carlo simulation to consider the statistics of irradiation from randomly-distributed potassium isotopes. This differs from the present work which is analytical, using a master equation, and which considers uniform radiation sources.

A key result is that the statistical properties of thermoluminescence can depend strongly on the geometrical shape of the sample. While the mean properties may remain unchanged, the statistical noise can vary dramatically depending of the relative orientation of the sample to the radiation source. A cylindrical sample, for example, can have completely different statistical behaviors depending on whether the source of the radiation is on the axis or transverse to it. This effect will be quantified for some model geometries.

To define terminology and provide a point of reference, the next section presents the usual phenomenological model of irradiation of a one-trap one-center system. Then the master equation will be developed for three cases of the same physical system and we will show how statistical properties, such as standard deviation, skewness, and kurtosis, can be derived. To obtain quantitative results, a model of energy deposition during irradiation is needed. This is developed in Section 4 using the Bethe theory with some simplifying assumptions. In Section 5, the irradiation model is combined with the master equation results to find the statistical properties of irradiated samples of differing shapes and orientations. This is followed by a section containing several example calculations illustrating how quick and simple estimates of standard deviations and other statistical properties can be computed. The strengths and limitations of this approach are summarized in the last section.

2. Phenomenological model

While the statistical properties will be developed in later sections, we will first review the phenomenological model of the irradiation process. A simple model consisting of one electron trap and one recombination center will be considered. This is illustrated in Fig. 1 where the electron trap has a concentration of N (cm^{-3}) with an occupation of n (cm^{-3}), and the recombination center has a concentration of M (cm^{-3}) with an occupation of m (cm^{-3}). A_m (cm^3/s) is the rate constant for recombination of free electrons with the center. B (cm^3/s) is the rate constant for trapping of free holes in the center. The corresponding phenomenological equations are:

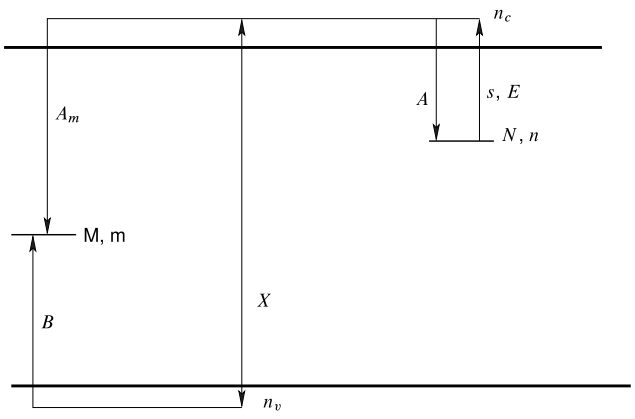

Fig. 1. Energy level diagram of the model with an active trap N and a hole recombination center M. During irradiation, electron–hole pairs are created with rate X. During heating, the electrons in trap N are thermally-excited, with a rate controlled by s, E, and recombine with the holes in M.

$$\frac{dn}{dt} = A(N-n)n_c \tag{1}$$

$$\frac{dn_c}{dt} = X - A(N-n)n_c - A_m m n_c \tag{2}$$

$$\frac{dm}{dt} = B(M-m)n_v - A_m m n_c \tag{3}$$

$$\frac{dn_v}{dt} = X - B(M-m)n_v \tag{4}$$

where X (cm^{-3}/s) is the rate at which radiation creates electron–hole pairs, n_c (cm^{-3}) is the concentration of free electrons, n_v (cm^{-3}) is the concentration of free holes, and t (s) is time. We will assume that initially, at $t = 0$, before irradiation starts, the trap and center are empty:

$$n = 0 \qquad \text{at } t = 0 \tag{5}$$

$$m = 0 \qquad \text{at } t = 0 \tag{6}$$

Experimental measurements show that rate constants for capture for free electrons or holes in traps or centers typically have values in the range from 10^{-10} cm^3/s to 10^{-5} cm^3/s. Rose (1955) and Lax (1960) Typical trap or center concentrations of interest in TL range from 10^{12} cm^{-3} to 10^{17} cm^{-3}. Consequently, the lifetime of free electrons or free holes, which is often measured in microseconds, is typically far less than the time scale over which irradiation or heating occurs. It follows that:

$$\frac{1}{n_c}\frac{dn_c}{dt} \ll A(N-n) \qquad \text{and} \qquad \frac{1}{n_v}\frac{dn_v}{dt} \ll B(M-m) \tag{7}$$

This leads to the quasi-steady approximation which allows Eqs. (2) and (4) to be simplified to:

$$n_c = \frac{X}{A(N-n) + A_m m} \tag{8}$$

$$n_v = \frac{X}{B(M-m)} \tag{9}$$

When the quasi-steady approximation is valid, it follows that:

$$n_c \ll n \qquad \text{and} \qquad n_v \ll m$$

In this case and using Eqs. (8) and (9), we can simplify Eqs. (1) and (3) to:

$$\frac{dn}{dt} = \frac{A(N-n)}{A(N-n) + A_m m} X \tag{10}$$

$$m = n \tag{11}$$

Eqs. (10) and (11) with initial conditions Eqs. (5) and (6) are the governing equations that apply to arbitrary dose. For simplicity, we will also consider the case for which the dose is low enough that:

$$n \ll \frac{A}{A + A_m} N \tag{12}$$

In this case, Eq. (10) reduces to:

$$\frac{dn}{dt} = X \tag{13}$$

Eq. (13) can be integrated to find the trap concentration n as a function of time. Using initial conditions Eqs. (5) and (6) as well as Eq. (11), it follows that at low-dose:

$$m(t) = n(t) = \mathcal{D}(t) \tag{14}$$

where:

$$\mathcal{D}(t) = \int_0^t X(t')dt' \tag{15}$$

where t' is a variable-of-integration. The quantity $\mathcal{D}$ is the applied dose as measured in electron–hole pairs per unit volume. The relationship between $\mathcal{D}$ and the dose measured in units of Grays will be discussed later. Eq. (14) indicates that every ion-pair creation, which occurs at rate X, results in the capture of a free electron by the trap and a free hole by the center. This is a property of the one-trap one-center model in the low dose limit (Eq. (12)).

In sum, we have derived the equations for the growth of trap and center populations for a one-trap one-center system. At low dose, this leads to the particularly simple result, Eqs. (14) and (15), that trap population is proportional to dose. The phenomenological equations predict trap and center populations that grow deterministically. These equations cannot predict the statistical nature of trap and center populations. That will be addressed in the next section.

3. Master equations

For small samples or small doses, the statistical nature of irradiation and recombination can become important. In this section, we develop master equations which govern the statistical behavior of samples irradiated by high-energy particles. In particular, the probability distributions for trap populations will be predicted. In the following three subsections, this is done for three different radiation models. We will also explore how these distributions connect to the conventional phenomenological equations.

Unlike the phenomenological model, it will matter here what type of irradiation is applied. In Lawless et al. (2020), it was assumed that one irradiation event results in one electron–hole pair as is typical of UV irradiation but not of irradiation by high-energy sources such X-rays or beta rays. Here, we consider high-energy sources.

Let us consider a sample of volume V and, within this volume, it has $\mathbb{M}$ centers and $\mathbb{N}$ traps. $\mathbb{M}$ and $\mathbb{N}$ are integers and are connected to the macroscopic quantities M and N via:

$$M = \mathbb{M}/V \qquad \text{and} \qquad N = \mathbb{N}/V \tag{16}$$

Let P_i be the probability that a sample, which might be a single grain, has exactly i electrons in its $\mathbb{N}$ traps at some time t. Because P_i is a probability, we will require that:

$$\sum_{i=0}^{\mathbb{N}} P_i = 1 \tag{17}$$

In the first subsection that follows, we will develop solutions for the probabilities P_i as a function of time first for a simple model which illustrates the key characteristics but admits analytical solutions. After this, a subsection is devoted to a more general model. While full solution of this model typically requires numerical methods, we will find analytical solutions for means, standard deviations and higher moments of its probability distribution. A third subsection addresses a special case which admits analytical solutions over the whole range from low dose to high dose.

3.1. Simple model

Consider the case where each ionizing ray generates exactly G_* electron–hole pairs in its track as it passes through the sample, such as a single grain, where G_* is a fixed number. If we keep the definition of X the same as in the macroscopic model, then, in a sample of volume V, we have tracks occurring at the rate of XV/G_* per second.

While the phenomenological model of Section 2 was concerned with *average* ionization rates, the master equation model of interest here requires knowledge of individual ionization events and how they affect the distribution of trap population probabilities, P_i. The first step is consider a very short (infinitesimal) time interval dt. Over this time, the material will experience either be subject to zero or one radiation tracks.[1] If zero tracks occur, then no ionization happens over this interval. If one track is incident, then G_* ionizations occur.

If we restrict the model to low dose as we did for the phenomenological model, then every free electron is captured by one of the $\mathbb{N}$ traps. It follows that the two ways that P_i may change over some small time interval, dt, are:

1. It could be that the sample has exactly $i - G_*$ electrons in the traps and then an ionization event that results in an increase in trap population to i occurs. For a sample of volume V that is subjected to irradiation at rate X, this causes P_i to increase by $(XV/G_*)P_{i-G_*}dt$. This applies to all trap populations i for which $i \geq G_*$.
2. It could be that the sample has exactly i electrons in the traps and then an ionization event occurs that results in an increase in trap population from i to $i + G_*$. This causes P_i to decrease by $(XV/G_*)P_i dt$. This applies for all possible trap populations i.

Combining these two possible events together, we have the master equation for low dose:

$$\frac{dP_i}{dt} = \begin{cases} -(XV/G_*)P_i & \text{for } 0 \leq i < G_* \\ (XV/G_*)P_{i-G_*} - (XV/G_*)P_i & \text{for } G_* \leq i \end{cases} \tag{18}$$

The second line in Eq. (18) is for $i \geq G_*$ and thus both scenarios as above are included. For the first line in Eq. (18) which applies to $i < G_*$, only the second scenario is included.

In order that both Eqs. (17) and (18) be obeyed at all times, it is necessary that:

$$\sum_{i=0} \frac{dP_i}{dt} = 0 \tag{19}$$

Note that every positive term in Eq. (18) for some i is balanced by an equal negative term for other i. Consequently, Eq. (18) obeys Eq. (19) and, therefore, if the initial conditions are chosen to obey Eq. (17), then Eq. (17) will also be obeyed at all times.

It is often assumed as an initial condition in thermoluminescence problems that the traps are empty. We would express that in terms of P_i by:

$$P_i(t = 0) = \begin{cases} 1 & \text{for } i = 0 \\ 0 & \text{for } i > 0 \end{cases} \tag{20}$$

For this initial condition, the master equation Eq. (18) has an exact solution in the form of a modified Poisson distribution:

$$P_i = \begin{cases} \frac{(V\mathcal{D}/G_*)^{i/G_*}}{(i/G_*)!} e^{-V\mathcal{D}/G_*} & \text{for } i = jG_* \text{ for integer } j \\ 0 & \text{otherwise} \end{cases} \tag{21}$$

[1] Since dt is assumed infinitesimally small, the chance of two or more rays arriving is negligible. This is the nature of a Poisson Process and further discussion can be found in statistics textbooks.

where V is the sample volume and D is the dose as defined in Eq. (15). The *expected value* of the trap population is defined by:

$$\mathbb{E}[i] = \sum_i i P_i \tag{22}$$

Substituting Eq. (21) into Eq. (22), we find the expected value of the trap population as a function of dose:

$$\mathbb{E}[i] = V D \tag{23}$$

$\mathbb{E}[i]$ is the expected total number of trapped electrons in the sample. (More details on the derivation of the statistical properties of the fixed-G model are given in Appendix A.) The number of trapped electrons per unit volume is:

$$\frac{\mathbb{E}[i]}{V} = D \tag{24}$$

Comparing Eq. (24) with Eq. (14), it is clear that the quantity n in the phenomenological equations should be identified with the statistical *expected value* of trapped electrons per unit volume:

$$n \equiv \frac{\mathbb{E}[i]}{V} \tag{25}$$

Unlike the phenomenological model, Eq. (21) can give us information on the statistical variation of trap population. The standard deviation, σ, of the trap population is defined by:

$$\sigma^2 = \sum_{i=0} \left(i - \mathbb{E}[i]\right)^2 P_i \tag{26}$$

From Eq. (21), the standard deviation can be found to be:

$$\sigma = \sqrt{G_* \mathbb{E}[i]} \tag{27}$$

A common way to characterize the relative size of a standard deviation is to compare its square to the expected value of the population. This ratio is called *dispersion*. In our case:

$$\mathbb{D} = \frac{\sigma^2}{\mathbb{E}[i]} = G_* \tag{28}$$

For many distributions commonly considered in statistics, including the usual Poisson distribution, $\mathbb{D} = 1$ or, at least, $\mathbb{D}$ is of order 1. It is important to note here that, since G_* may be quite large, the dispersion $\mathbb{D}$ may also be quite large.

The phenomenological model was developed under the low dose assumption as expressed by Eq. (12). For the master equation, the low dose assumption is expressed analogously: any P_i with a significant (large) value is for an i that is small enough that:

$$i \ll \frac{A}{A + A_m}\mathbb{N} \qquad \text{for any } i \text{ for which } P_i \text{ is significant} \tag{29}$$

In addition to limiting dose, Eq. (29) implies limit on G_*: $G_* \ll \frac{A}{A+A_m}\mathbb{N}$.

In sum, we have considered the low-dose limit of the simple case where each ray (or track) produces exactly G_* electron–hole pairs. The predicted mean trap population is the same as predicted by the phenomenological model, Eq. (14). The standard deviation in the trap population, however, is proportional to $\sqrt{G_*}$. For the special case of UV irradiation with $G_* = 1$, the standard deviation agrees with our earlier result (Lawless et al., 2020). For irradiation by high-energy particles, such as alpha or beta rays, we shall see that values of G_* may be orders of magnitude larger than 1.

3.2. Variable G: A more general model

It is more typical that the number of electron–hole pairs produced in a sample by an incident ionizing ray may vary widely from one ray to the next. We will consider that case here and this will produce results that are similar to but more general than those of the preceding subsection.

Let us let the expected number of rays per unit time incident on our sample be $\mathbb{X}$ (s^{-1}). Let the probability that a ray produces G electron–hole pairs be f_G. f_G will depend on the type of ray, the energy of the ray, and the geometry and material properties of the sample. If we consider the probability P_i that the material has exactly i filled traps, there are two reasons why P_i might change:

1. There is a chance that the material could have some lower number of trapped electrons, say $i - G$, and, over a short time interval dt, a ray that passes through the material and generates exactly G electron–hole pairs. This would cause P_i to increase by $f_G \mathbb{X} P_{i-G} dt$.
   Note that, in this scenario, the initial number of trapped electrons is $i-G$. Since the initial number of trapped electrons cannot be negative, this scenario only apples when $i \geq G$.
2. If the material currently has i filled traps, there is a chance that, over a short time interval dt, a ray passes through the material causing the creation of G electron–hole pairs. For each G this reduces the P_i by $f_G \mathbb{X} P_i dt$ and the total effect on P_i is the sum over all possible G.

Thus, our master equation becomes:

$$\frac{dP_i}{dt} = \sum_{G=0}^{i} f_G \mathbb{X} P_{i-G} - \sum_{G\geq 0} f_G \mathbb{X} P_i \tag{30}$$

The first sum on the right-hand-side of Eq. (30) refers to excitation from $i-G$ trapped electrons to i trapped electrons. Since the initial number of electrons can never be negative, the limits on the sum are set to ensure that $i - G$ is nonnegative.

Since f_G is a probability, we require that:

$$\sum_{G\geq 0} f_G = 1 \tag{31}$$

The assumption underlying Eq. (30) is that, if radiation creates G electron–hole pairs, then the trap and center populations increase by G. This is true only at low enough dose that capture of the free electron by the trap is much more probable than its recombination with the center. While, in principle, the sum over "$i \geq 0$" extends from $i = 0$ to $i = \mathbb{N}$, the low dose approximation requires that P_i become negligibly small before i approaches $\mathbb{N}$. In a phenomenological model, low dose assumption is expressed by Eq. (12). For the master equation approach, it is expressed by the analogous requirement that the dose is low enough that P_i is negligibly small for large i as per Eq. (29).

Examination of Eq. (30) will also show that solutions obeying Eq. (29) are only possible if f_G becomes zero or at least negligibly small for large G. We will make quantitative estimates for f_G in Section 4 and provide sample calculations of P_i in Section 6 showing that this requirement is easy to meet. For completeness, the opposite limiting case where large G values dominate is taken up in Section 3.3 and also discussed in Section 4.

The first important property to determine is the rate of change of the mean trap population. Combining Eqs. (22) and (30), we have:

$$\frac{d\mathbb{E}[i]}{dt} = \sum_{i\geq 0} i \frac{dP_i}{dt} \tag{32}$$

$$= \mathbb{X} \sum_{i\geq 0} \sum_{G=0}^{i} f_G i P_{i-G} - \mathbb{X} \sum_{i\geq 0} \sum_{G\geq 0} f_G i P_i \tag{33}$$

Continuing on from Eq. (33) and rearranging the summation using the method detailed in Appendix C, we find:

$$\frac{d\mathbb{E}[i]}{dt} = \mathbb{X} \sum_{G\geq 0} \sum_{i\geq 0} f_G (i+G) P_i - \mathbb{X} \sum_{G\geq 0} \sum_{i\geq 0} f_G i P_i \tag{34}$$

$$= \mathbb{X} \sum_{G\geq 0} \sum_{i\geq 0} f_G G P_i \tag{35}$$

$$= \mathbb{X} \sum_{G\geq 0} \left(f_G G\right) \sum_{i\geq 0} P_i \tag{36}$$

$$= \mathbb{X}\overline{G} \tag{37}$$

where $\overline{G}$ is defined by:

$$\overline{G} = \sum_{G\geq 0} f_G G \tag{38}$$

Since $\mathbb{X}$ is the average number of rays per unit time that pass through the sample and $\overline{G}$ is the average number of electron–hole pairs produced for those rays, it follows that:

$$XV = \mathbb{X}\overline{G} \tag{39}$$

This means that Eq. (37) can also be written as:

$$\frac{d\mathbb{E}[i]}{dt} = XV \tag{40}$$

Combined with initial condition Eq. (20), Eq. (40) can be immediately integrated to find the growth in the expected trap population with exposure time:

$$\mathbb{E}[i] = V\mathcal{D}(t) \tag{41}$$

where $\mathcal{D}(t)$ is the ionization dose (cm^{-3}) accumulated as of time t and is defined by Eq. (15). We will later develop the connection between the dose $\mathcal{D}$ (electron–hole pairs per unit volume) which is commonly used in theoretical studies and the dose $\mathcal{D}_G$, measured in Grays, which is commonly used in experimental work. If we identify n as the expected value of trap population per unit volume:

$$n = \mathbb{E}[i]/V \tag{42}$$

Eq. (40) becomes:

$$\frac{dn}{dt} = X \tag{43}$$

Eq. (43) agrees with Eq. (10) which shows that the n in the phenomenological equations should be interpreted as the statistical expected value of trap concentration.

To understand the reproducibility of experiments, it is helpful to know the standard deviation and other properties of the trap population distribution. To do this, we start by defining the k-th central moment of the distribution as:

$$\mu_k = \sum_{i\geq 0} \left(i - \mathbb{E}[i]\right)^k P_i \tag{44}$$

From the definition of μ_k in Eq. (44) and the definition of standard deviation σ (Eq. (26)), it is clear that:

$$\sigma^2 = \mu_2 \tag{45}$$

Combining Eq. (44) with the master Eq. (30) and after much algebra (see Appendix B), we find:

$$\frac{d\sigma^2}{dt} = \mathbb{X}\overline{G^2} \tag{46}$$

where $\overline{G^2}$ and all higher raw moments of G are defined by:

$$\overline{G^k} = \sum_{G\geq 0} f_G G^k \tag{47}$$

From the identity $\mathbb{X}\overline{G} = XV$, Eq. (46) becomes:

$$\frac{d\sigma^2}{dt} = \frac{\overline{G^2}}{\overline{G}} XV \tag{48}$$

If we start from empty traps at $t = 0$ (Eq. (20)), then Eq. (48) integrates to:

$$\sigma^2 = \frac{\overline{G^2}}{\overline{G}} V\mathcal{D} \tag{49}$$

or, using Eq. (41):

$$\sigma^2 = \frac{\overline{G^2}}{\overline{G}} \mathbb{E}[i] \tag{50}$$

The index of dispersion is found by taking the ratio of Eq. (50) to Eq. (41):

$$\mathbb{D} = \frac{\sigma^2}{\mathbb{E}[i]} = \frac{\overline{G^2}}{\overline{G}} \tag{51}$$

Just as for the fixed-G_* model of Section 3.1, it is possible for the dispersion in Eq. (51) to be much larger than one.

As dose increases, the trap population distribution will approach a Gaussian distribution. Since we know the mean, Eq. (37), and the standard deviation, Eq. (49), we have all the parameters needed to fully specify a Gaussian distribution. Our focus, however, is on low doses and the Gaussian distribution may not apply. In later sections, we will show that, at low doses, the distribution of trap population is not Gaussian, and not even approximately Gaussian. For low dose, thus, it is helpful to know more moments.

The third central moment of the distribution, μ_3, quantifies the asymmetry of the distribution. As derived in the appendix, Eq. (B.14), grows as:

$$\frac{d\mu_3}{dt} = \mathbb{X}\overline{G^3} \tag{52}$$

If we again assume initially empty traps (Eq. (20)), this integrates to:

$$\mu_3 = \frac{\overline{G^3}}{\overline{G}} V\mathcal{D} \tag{53}$$

When μ_3 is commonly normalized by the cube of standard deviation and the result is called Pearson's moment coefficient of skewness, $\widetilde{\mu_3}$:

$$\widetilde{\mu_3} = \frac{\mu_3}{\sigma^3} \tag{54}$$

Combining Eq. (49) with Eq. (53)

$$\widetilde{\mu_3} = \frac{\overline{G^3}}{\overline{G^2}^{3/2}} \overline{G}^{1/2} (V\mathcal{D})^{-1/2} \tag{55}$$

We see that skewness starts out large and positive, indicating the distribution is highly asymmetric and has a larger tail on the positive side than on the negative side of the mean. Eq. (55) shows that skewness declines as dose increases. For comparison, a normal (Gaussian) distribution has zero skewness.

Like the second central moment, the fourth central moment of the distribution reflects the width but is more sensitive to the tails of the distribution. As derived in the appendix (Eq. (B.15)), the fourth central moment of the distribution grows as:

$$\frac{d\mu_4}{dt} = \mathbb{X}\left(6\overline{G^2}\sigma^2 + \overline{G^4}\right) \tag{56}$$

Again starting from empty traps (Eq. (20)), and using Eq. (49), Eq. (56) can be integrated to find:

$$\mu_4 = 3\left(\frac{\overline{G^2}}{\overline{G}} V\mathcal{D}\right)^2 + \frac{\overline{G^4}}{\overline{G}} V\mathcal{D} \tag{57}$$

If we normalized μ_4 by the standard deviation, we obtain Pearson's kurtosis coefficient, $\widetilde{\mu_4}$:

$$\widetilde{\mu_4} = \frac{\mu_4}{\sigma^4} \tag{58}$$

Substituting Eq. (57) into Eq. (58), we find

$$\widetilde{\mu_4} = 3 + \frac{\overline{G}\,\overline{G^4}}{\left(\overline{G^2}\right)^2 V\mathcal{D}} \tag{59}$$

If we think of the standard deviation as the width of the 'shoulders' of the distribution, then kurtosis measures the width of the tails of the distribution relative to the shoulders. Eq. (59) shows that the kurtosis starts very large, indicating wide tails, and decreases asymptotically to 3 at high dose. The kurtosis of the Gaussian distribution is 3.

As a special case of the above results, consider:

$$f_G = \begin{cases} 1 & \text{for } G = G_* \\ 0 & \text{for } G \neq G_* \end{cases} \tag{60}$$

For this special case, $\overline{G^n} = {G_*}^n$ and the results here for standard deviation, Eq. (49), and dispersion, Eq. (51), reduce to the corresponding results of the preceding subsection, Eqs. (27) and (28), respectively. In addition, for this case, the results above for skewness, Eq. (55), and kurtosis, Eq. (59) reduce to:

$$\widetilde{\mu_3} = \sqrt{\frac{G_*}{V\,D}} \tag{61}$$

$$\widetilde{\mu_4} = 3 + \frac{G_*}{V\,D} \tag{62}$$

In sum, equations for the statistical properties of the trap population after irradiation have been developed. These results apply at low-dose, Eq. (12), and allow for a variable number, G, of electron–hole pairs produced by each incident ray. While the *expected value* population again agrees with the phenomenological model, these equations can also predict the complete probability distribution of trap population after irradiation. Simple formulas are found for standard deviation, Eq. (49), dispersion, Eq. (51), and the higher central moments including skewness, Eq. (55), and kurtosis, Eq. (59). All these properties depend on the mean value of G, $\overline{G}$, and on its higher raw moments, $\overline{G^n}$. Numerical values for $\overline{G}$ and $\overline{G^n}$ can be estimated using the results to be found in Section 4 and Section 5.

3.3. Large G at arbitrary dose

In the preceding subsections, we assumed that the typical number of electrons freed by a single ray, G, was much smaller than the number of traps in the sample, $\mathbb{N}$. For completeness, we will consider the opposite case here where $G \gg \mathbb{N}$. The approach here also differs from the previous two subsections in that it does not assume a low dose: the solution developed here is valid for all doses, from low to high.

The assumption here is that every incident ray produces enough free electrons, G, to more than fill all the $\mathbb{N}$ traps with any electrons left over recombining at the center. Let $\mathbb{X}$ be the number of such rays per unit time incident on the sample. Thus, if there is some probability P_i that i traps are filled, where $0 \le i \le \mathbb{N}-1$, at time t, then, after some short time interval, dt, P_i will decrease by $\mathbb{X}P_i dt$ and the probability that all the traps are full, that is P_i with $i = \mathbb{N}$, increases by a corresponding amount. The total increase in the probability that all traps are full will be the sum of these individual contributions from i in the range $0 \le i \le \mathbb{N}-1$. Thus, the master equation becomes:

$$\frac{dP_i}{dt} = \begin{cases} -\mathbb{X}P_i & \text{for } 0 \le i < \mathbb{N} \\ \sum_{j=0}^{\mathbb{N}-1} \mathbb{X}P_j & \text{for } i = \mathbb{N} \end{cases} \tag{63}$$

where $\mathbb{X}$ is the number of rays per unit time incident on the sample. Assuming that the traps are initially empty, Eq. (20), the solution to Eq. (63) is:

$$P_i = \begin{cases} \exp(-\mathbb{X}t) & \text{for } i = 0 \\ 0 & \text{for } 0 < i < \mathbb{N} \\ 1 - \exp(-\mathbb{X}t) & \text{for } i = \mathbb{N} \end{cases} \tag{64}$$

It follows that the expected value of the trap population is:

$$\mathbb{E}[i] = \sum_i i P_i = \mathbb{N}\left[1 - \exp(-\mathbb{X}t)\right] \tag{65}$$

Again using Eq. (64), we can immediately find the k^{th} central moment of the distribution:

$$\mu_k = \sum_{i=0} \left(i - \mathbb{E}[i]\right)^k P_i \tag{66}$$

$$= \mathbb{N}^k \left[(\exp(-\mathbb{X}t) - 1)^k \exp(-\mathbb{X}t) + (\exp(-\mathbb{X}t))^k \left(1 - \exp(-\mathbb{X}t)\right)\right] \tag{67}$$

Or, using Eq. (65), Eq. (67) can be rewritten as:

$$\mu_k = \left(1 - \frac{\mathbb{E}[i]}{\mathbb{N}}\right)\left(-\mathbb{E}[i]\right)^k + \left(\frac{\mathbb{E}[i]}{\mathbb{N}}\right)\left(\mathbb{N} - \mathbb{E}[i]\right)^k \tag{68}$$

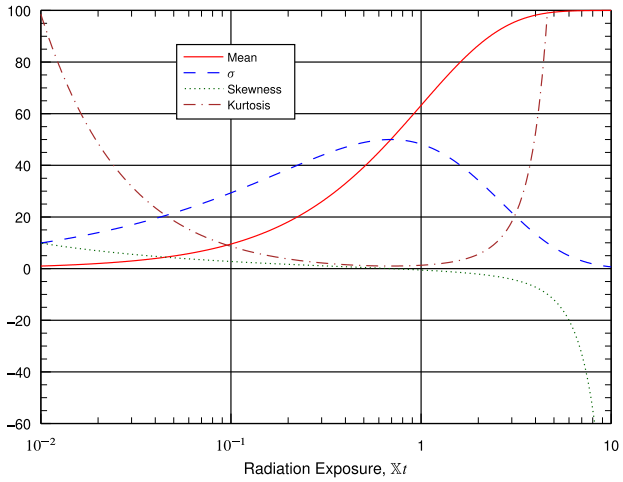

Fig. 2. The expected value $\mathbb{E}[i]$ (Eq. (65)), standard deviation σ (Eq. (69)), skewness (Eq. (73)), and kurtosis (Eq. (76)) of the large G solution are shown as a function of radiation exposure. Both $\mathbb{E}[i]$ and σ scale linearly with the number of traps in the sample, $\mathbb{N}$. The curves shown were computed for $\mathbb{N} = 100$. The curves for skewness and kurtosis are independent of $\mathbb{N}$.

To find the standard deviation, σ, we take the square root of the second central moment, μ_2:

$$\sigma = \sqrt{\mu_2} = \mathbb{N}\sqrt{(1 - \exp(-\mathbb{X}t))\exp(-\mathbb{X}t)} \tag{69}$$

Or, using Eq. (68):

$$\sigma = \sqrt{\mathbb{E}[i]\left(\mathbb{N} - \mathbb{E}[i]\right)} \tag{70}$$

It follows that the dispersion is:

$$\mathbb{D} = \mathbb{N} - \mathbb{E}[i] \tag{71}$$

Since $\mathbb{N}$ tends to be very large, the dispersion starts large at low dose and remains large up until saturation, $\mathbb{E}[i] \to \mathbb{N}$, is approached.

The asymmetry of the distribution, as given by Pearson's moment coefficient of skewness, is:

$$\widetilde{\mu_3} = \frac{\mu_3}{\sigma^3} \tag{72}$$

$$= \frac{2\exp(-\mathbb{X}t) - 1}{\left[\exp(-\mathbb{X}t)\left(1 - \exp(-\mathbb{X}t)\right)\right]^{1/2}} \tag{73}$$

Or, using Eq. (68):

$$\widetilde{\mu_3} = \frac{\mathbb{N} - 2\mathbb{E}[i]}{\sqrt{\mathbb{E}[i]\left(\mathbb{N} - \mathbb{E}[i]\right)}} \tag{74}$$

From Eq. (74), we see that skewness is very large and positive at low dose, for which $\mathbb{E}[i] \ll \mathbb{N}$, and very large and negative at high dose, for which $\mathbb{E}[i] \to \mathbb{N}$. Skewness is zero when $\mathbb{E}[i] = \mathbb{N}/2$.

Using Eq. (67), kurtosis, which measures the relative tail width, is:

$$\widetilde{\mu_4} = \frac{\mu_4}{\sigma^4} \tag{75}$$

$$= \frac{1 - 3\exp(-\mathbb{X}t) + 3\exp(-2\mathbb{X}t)}{\exp(-\mathbb{X}t)\left(1 - \exp(-\mathbb{X}t)\right)} \tag{76}$$

Using Eq. (68), this becomes:

$$\widetilde{\mu_4} = \frac{\left(\mathbb{E}[i]/\mathbb{N}\right)^2}{1 - \mathbb{E}[i]/\mathbb{N}} + \frac{\left(1 - \mathbb{E}[i]/\mathbb{N}\right)^2}{\mathbb{E}[i]/\mathbb{N}} \tag{77}$$

Similar to skewness, kurtosis becomes very large at either low dose or high dose. At $\mathbb{E}[i] = \mathbb{N}/2$, kurtosis reaches a minimum value of 1 which is the lowest possible kurtosis for any distribution. For comparison, the kurtosis of a Gaussian distribution is 3.

Table 1
Statistical properties of the three models of irradiation: fixed-G, variable-G, and large-G. The results of the large-G model are shown both in the general form, as derived in Section 3.3 and its low-dose limit for which the other two models are valid.

Model:	Fixed G (Section 3.1)	Variable G (Section 3.2)	Large G	Large G (Section 3.3)
Dose range:	Low	Low	Low	Any
Expected value, $\mathbb{E}[i]$	$V\mathcal{D}$	$V\mathcal{D}$	$(\mathbb{N}/\overline{G})V\mathcal{D}$	$\mathbb{N}\left(1-\exp(-\mathcal{D}/\overline{G})\right)$
Standard deviation, σ	$\sqrt{G_*\mathbb{E}[i]}$	$\sqrt{\left(\overline{G^2}/\overline{G}^2\right)\overline{G}\mathbb{E}[i]}$	$\sqrt{\mathbb{N}\mathbb{E}[i]}$	$\sqrt{\mathbb{E}[i]\left(\mathbb{N}-\mathbb{E}[i]\right)}$
Dispersion, $\mathbb{D}$	G_*	$\overline{G^2}/\overline{G}$	$\mathbb{N}$	$\mathbb{N}-\mathbb{E}[i]$
Skewness, $\widetilde{\mu_3}$	$\sqrt{G_*/\mathbb{E}[i]}$	$\left(\overline{G^3}/\overline{G^2}^{3/2}\right)\sqrt{\overline{G}/\mathbb{E}[i]}$	$\sqrt{\mathbb{N}/\mathbb{E}[i]}$	$\frac{\mathbb{N}-2\mathbb{E}[i]}{\sqrt{\mathbb{E}[i]\left(\mathbb{N}-\mathbb{E}[i]\right)}}$
Kurtosis, $\widetilde{\mu_4}$	$G_*/\mathbb{E}[i]+3$	$\left(\overline{G^4}/\overline{G^2}^2\right)\left(\overline{G}/\mathbb{E}[i]\right)+3$	$\mathbb{N}/\mathbb{E}[i]-2$	$\frac{\left(\mathbb{E}[i]/\mathbb{N}\right)^2}{1-\mathbb{E}[i]/\mathbb{N}}+\frac{\left(1-\mathbb{E}[i]/\mathbb{N}\right)^2}{\mathbb{E}[i]/\mathbb{N}}$

In Fig. 2, the various statistical properties of the large-G model are plotted against the radiation exposure, $\mathbb{X}t$. $\mathbb{X}t$ can also be interpreted as the statistically expected number of rays that the material has experienced. To illustrate, let us consider $\mathbb{X}t = 0.1$. Since the arrival of rays of radiation is a Poisson process, this means that there is a 9.05% chance of the material experiencing exactly one ray over this time, a 0.45% chance of it experiencing exactly two rays, and so on, with a total chance of 9.52% that *one or more* rays arrive. Consequently, if this experiment was repeated a large number of times, we would expect 9.52% of the experiments to show full traps at the end and $100 - 9.52 = 90.48\%$ to show empty traps. Thus, for a material with $\mathbb{N} = 100$ total traps, we would expect the experimentally-measured mean trap concentration after irradiation to tend toward 9.52 and this matches the value of $\mathbb{E}[i]$ derived from Eq. (65) and as shown in Fig. 2. The standard deviation in the number of filled traps that one would measure after these experiments is 29 which is larger than the mean. The standard deviation is shown by the dashed line in Fig. 2. The kurtosis is 8.6, indicating wide tails in the distribution of results. The skewness is positive, 2.76, indicating that the tails in the measured trap population skew to the high side.

The applicability of the large-G model, which requires $\mathbb{N} \ll \overline{G}$, is likely limited to small and very pure samples subjected to a high energy but short-range radiation. These requirements on the material and radiation will be considered further in Section 4.

3.4. Summary

The similarity and differences between the three models are highlighted in Table 1. For each model, it is found that the statistical properties of the irradiated sample depend strongly on the number G of electron–holes pairs created per ray of radiation. Each model makes different assumptions about G. Unlike the other two, the large-G model of Section 3.3 is valid over the full low through the high dose range. To make it easier to see the parallelism between the models, the large-G results are also shown in Table 1 in the low-dose limit. The expected number of trapped electrons after irradiation, $\mathbb{E}[i]$, is the same for the fixed-G and variable-G models. The large-G model predicts a smaller number of trapped electrons because, in this model, many of the radiation-produced electron–hole pairs result in recombination, not trapping. All three models predict a standard deviation of trap population that, in the low dose limit, scales with the square root of the trap population and a dispersion that depends on the type of radiation but not the dose. We will find in a later section that, for common geometries, the factors $\overline{G^2}/\overline{G}^2$, $\overline{G^3}/\overline{G^2}^{3/2}$ and $\overline{G^4}/\overline{G^2}^2$ which appear in the variable G model are all of order one.

4. Irradiation model

The results of the previous section allow the determination of the statistical behavior of irradiated materials if the values of the probabilities f_G are known. To proceed further, we need estimates of f_G and this requires a model of the irradiation process and knowledge of the geometry of the thermoluminescent grain or sample. We will address the irradiation model in this section and the geometry in the next. For irradiation by alpha or beta rays, Bethe theory, along with some simplifying assumptions, will be used. There are two steps discussed in this section: the first is to quantify stopping power and the second is to convert stopping power to electron–hole pair production rate.

Table 2
Data for common TL materials. (Attix, 2004; Wilson et al., 1982; ICRU, 1984; Berger et al., 2005).

Material	$n_A Z/\rho$ (10^{23} g^{-1})	I (eV)
CaF_2	2.93	166
LiF	2.79	94
NaI	2.571	452
SiO_2	3.01	139
Al_2O_3	2.95	145

For the first step, consider a particle of radiation as it travels through a material and loses energy. The rate of energy loss per unit distance is called *stopping power*, S_P. For beta rays, the electronic stopping power as given by Bethe's theory is: (Dalgarno, 1962)

$$S_\mathrm{P} \equiv -\frac{dT}{dx} = 2\pi\left(\frac{e^2}{4\pi\epsilon_0}\right)^2 \frac{n_A Z}{m_e v^2}\left[\ln\left(\frac{m_e v^2 T}{2I^2(1-(v/c)^2)}\right) - \left(2\sqrt{1-(v/c)^2} - 1 + (v/c)^2\right)\ln 2 + 1 - (v/c)^2 + \frac{1}{8}\left(1-\sqrt{1-(v/c)^2}\right)^2\right] \tag{78}$$

where T is the particle kinetic energy (J) and x (m) is the distance traveled. e is charge of an electron (Coulombs), ϵ_0 is the permittivity of free space (C/V/m), n_A is the number density of atoms in the target material (m^{-3}), Z is the number of electrons per atom in the target material, m_e is the electron rest mass (kg), v is the speed of particle of radiation (m/s), c is the speed of light (m/s), I is the logarithmic mean of atomic excitation energies (J) weighted by oscillator strength in the material. Thus, stopping power is a function of the properties of both the incident particle and the target material. For typical beta sources, the relativistic corrections, terms involving v/c, are important. The relationship between v and T is given by:

$$v = c\sqrt{1-\frac{1}{(1+T/m_e c^2)^2}} \tag{79}$$

Tabulated values of stopping powers for beta rays are available (ICRU, 1984). This can also be conveniently accessed online (Berger et al., 2005).(see Table 2). .

The second step is to relate the energy loss to the creation rate of electron–hole pairs (Attix, 2004; Arshak and Korostynska, 2006; Ryan, 1973; Scholze et al., 1998; Alig and Bloom, 1975; Klein, 1968; Goldstein, 1965; Barnett et al., 2013). The energy lost by the incident

Table 3
Energy per ion pair, W, for pure samples of various materials of interest. (Attix, 2004; Arshak and Korostynska, 2006; Ryan, 1973; Scholze et al., 1998).

Material	W (eV)
Si	3.6
Ge	2.8
GaAs	4.8
SiO_2	17
CdTe	4.4

particle to excitation of atomic electrons can take many forms. The excited electrons can be valence electrons or inner shell. The electron may be excited to a higher state or it may be freed. The freed electrons, called secondary electrons, are generally superthermal and may have enough energy to travel and ionize further electrons. The decay of highly excited states may release photons which travel further and cause subsequent ionizations. For our purposes, the important parameter is the ratio of energy deposited to number of electron–hole pairs created. This ratio, called W, is found to depend strongly on the material but, at least for high-energy radiation, only weakly on the type of radiation. Consequently, if $-dT/dx$ is the loss of energy to electronic excitation of a ray per unit distance, then the number of electron–hole pairs created per unit distance traveled by each ray is:

$$-\frac{1}{W}\frac{dT}{dx} \tag{80}$$

To find the total number of electron–hole pairs created by the ray, we can integrate:

$$G = \frac{1}{W}\int_0^{\min(R,L)} \left(-\frac{dT}{dx}\right) dx \tag{81}$$

where dx is an element of distance that the ray traverses. The upper limit of integration is the total distance the ray travels which is either the distance, L, that the ray travels from entry until it exits the material, or if the ray does not exit, the range R that it travels before stopping. The distance L of course depends on where the ray enters the sample and the direction of the ray relative to the sample.

Beta rays can be deflected during their travel through a material with the result that the path traveled to reach a particular penetration depth into a material is larger than that penetration depth. The ratio of the penetration depth to actual path length (or, in some literature, its inverse) is called the *detour factor*. For electrons emitted by ^{90}Y, the detour factor in water is about 0.65 (Ljungberg and Sjögreen Gleisner, 2018; Fernández-Varea et al., 1996). The detour factor tends to be smaller, and therefore more important, for lower energy beta sources or higher-Z target materials. For detailed quantitative analysis of a particular experiment with a particular radiation source and target material, analysis may need to include the detour factor. For simplicity in this current study, we set the detour factor to one and assume the rays travel in straight lines.

For various beta ray energies and target materials, the ionizations per track, G, is plotted against material thickness in Fig. 3. For short lengths, G grows linearly with material thickness. As the material thickness increases, the ray's energy T decreases and, consequently, as per Eq. (78), the stopping power, $S_P \equiv -dT/dx$ increases, and G grows faster than linearly. After the range has been exceeded, the beta ray has deposited all of its energy and there is no further increase in G.

For an alpha ray, Bethe theory (Dalgarno, 1962) predicts the stopping power to be:

$$-\frac{dT}{dx} = 4\pi\left(\frac{ze^2}{4\pi\epsilon_0}\right)^2 \frac{n_A Z}{m_e v^2}\left[\ln\left(\frac{2m_e v^2}{I}\right) + \ln\left(\frac{1}{1-(v/c)^2}\right) - (v/c)^2\right] \tag{82}$$

where: z is the charge of incident particle (2 for an alpha ray) and other parameters are as above. The relationship between v and T is given by:

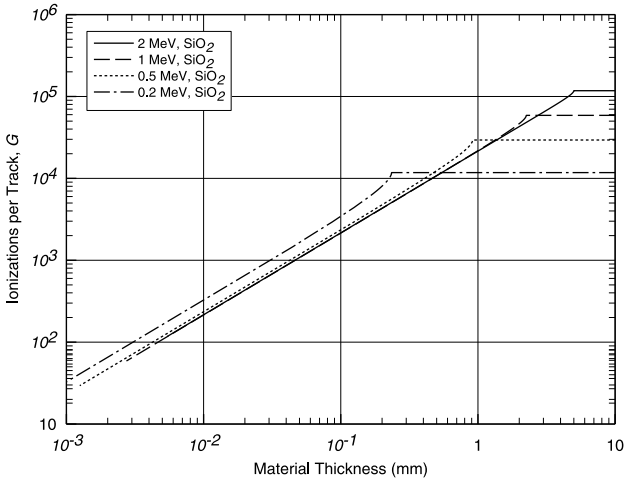

Fig. 3. The number of electron–hole pairs created per track, G, is plotted against material thickness for various beta ray energies and a target material of silica. A detour factor of one is assumed. A detour factor different from one would result in a larger number of ionizations for a given material thickness. The results here were calculated using Eq. (81) where the stopping power, $S_P = -dT/dx$, can be calculated using either Eq. (78) or the ESTAR database (Berger et al., 2005).

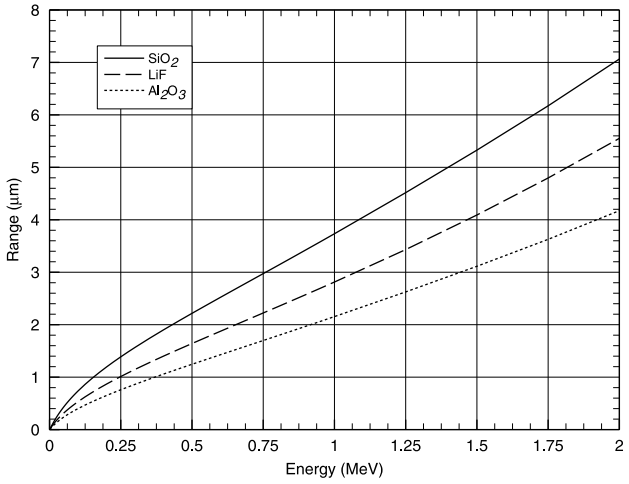

Fig. 4. The projected range of an alpha particle is plotted against the particle's initial energy for three different materials.

$$v = c\sqrt{1 - \frac{1}{(1 + T/m_\alpha c^2)^2}} \tag{83}$$

where m_α is the rest mass of the alpha particle, m_α=4 AMU. For typical alpha sources, the terms involving v/c are small and can be neglected. Tabulated values of stopping powers and ranges for alpha rays are available (Berger et al., 2005; ICRU, 1993). This can also be conveniently accessed online (Berger et al., 2005).

Bethe theory, Eq. (78) and (82), provides stopping power caused by collisions of the radiation with electrons in the target's atoms and molecules. This is the dominant source of stopping power over the range of typical interest in thermoluminescence. It should be noted, though, that for very low energy alpha rays, say $T < 10^{-2}$ MeV, collisions of the alpha ray with nuclei become important. For beta rays at high energies, say $T > 10$ MeV, energy loss to radiation becomes important.

A key difference between alpha and beta radiation is that, at typical energies, the order of 1 MeV, the range of alpha particles is orders of

magnitude shorter than that of beta particles. The projected range of alpha particles in various materials is shown in Fig. 4. The densities for SiO2, LiF, and Al2O3 were assumed to be 2.32 g/cm^3, 2.635 g/cm^3, and 3.97 g/cm^3 respectively. Samples with greater porosity (lower density) will have proportionally lower stopping powers and longer ranges. For the materials and ranges of energy shown, a sample of 10 μm or greater thickness will completely stop an alpha particle. Consequently, for samples of such thickness, the number of electron–hole pairs created by the alpha ray is simply:

$$G = T/W \tag{84}$$

In Section 3, models were considered for the limits of small-G and large-G. The theory in this section can be used to estimate which is more appropriate. As an example, consider a very pure sample, say $N \sim 10^{12}$ cm^{-3} with a linear dimension of $d \sim 10$ μm. Thus, $V \sim d^3 \sim 10^{-9}$ cm^3 and $\mathbb{N} \sim 10^{12} \times 10^{-9} \sim 10^3$. If it is subjected to alpha radiation, say $T \sim 1$ MeV, the radiation will be absorbed within the sample (see Fig. 4) and G can be estimated from Eq. (84). With $W \sim 10$ eV, we have $G \sim T/W \sim 10^5$. Thus $\mathbb{N} \ll G$ and the large-G model is appropriate in this case.

When looked at in detail, the ionization process is statistical. Thus, for a given material with characteristic W and a given ray of energy T, the actual number G of electron–hole pairs created will vary from one incident ray to the next. The dispersion of G due to this, however, is typically one or less (Klein, 1968) and consequently we will neglect it here.

The assumption of straight line paths for alpha rays is typically accurate. For beta rays, it is accurate for thin materials or higher energies rays and lower Z materials (Scott, 1963; Highland, 1975, 1979; Lynch and Dahl, 1991; Turner, 2007). A first estimate for the error caused assuming straight lines for beta rays might be obtained by considering the detour factor. A detour factor of 0.5, for example, would indicate that twice as much ionization was occurring in the material per unit depth in a slab-like geometry than the straight line model would predict. This leads to an increase in standard deviation and dispersion of the trap population. A better estimate would use a Monte-Carlo simulation of beta particle paths and ionization in the sample material and for the sample geometry (Kawrakow, 2000; Sood, 2017; Salvat et al., 2007; Nuclear Energy Agency, 2019; Nikjoo et al., 2006; Agostinelli et al., 2003; Allison et al., 2006) but that is beyond the scope of this article.

Lastly, the usual experimental unit of radiation is Gray where 1 Gray = 1 J/kg while the usual theoretical unit, such as D in Eq. (15), is ionizations per unit volume. The relationship between the two is:

$$\mathcal{D}_G = \frac{W}{\rho}\, \mathcal{D} \tag{85}$$

where W is again the average energy per ionization (Table 3) and ρ is the material mass density.

5. Sample geometry

A sample of thermoluminescent material, which may be as small as a single grain, may occur in a variety of shapes. Some sample shapes will be considered and, using the simplified radiation model of Section 4, the probability distribution f_G of the number of electron–hole pairs created by a single radiation track. Knowledge of the distribution f_G will enable calculation of the statistical properties of irradiation as described in Section 3.

To simplify the calculations, we consider two limiting cases, one for thick samples and one for thin samples relative to the range of a radiation particle. Thus, a thin sample is one for which the radiation track enters on one side and, with little change in energy, exits on another. A thick sample is one for which the particle of radiation is stopped within the material.

Suppose that a ray has energy T_0 when it enters the sample and energy T_1 at the end of its path through the sample. In that case, the number of electron–hole pairs created by the ray is:

$$G = \frac{T_0 - T_1}{W} \tag{86}$$

where W is the energy per electron–hole pair. For a thick sample, $T_1 = 0$. For a thin sample, the stopping power theory of Section 5.2 is needed to calculate T_1. These two cases will be considered in the next two subsections.

5.1. Thick sample

Consider the case where the penetration depth of the radiation is less than the sample thickness for which the number of electron–hole pairs created by each ray is given by Eq. (84). We can consider three cases:

- If we have low dose and $G \ll \mathbb{N}$ and monoenergetic radiation, then the number of electron–hole pairs is also the number of new trapped electrons and the model of Section 3.1 applies with $G_* = T/W$ where T is the energy of the radiation and W is the material's energy per electron–hole pair.
- If we have low dose and $G \ll \mathbb{N}$ and the radiation has a distribution of energies, as is typical of radioisotope sources, then the variable G theory of Section 3.2 can be applied. If f_T is the probability distribution of energy T, then, using Eq. (84), the distribution of G would be a scaled version of f_T: $f_G(G) = W f_T(WG)$.
- If $G \gg \mathbb{N}$, as might be the case of high energy radiation and tiny pure samples, then the theory of Section 3.3 applies. This theory applies over the complete range from low dose to high dose.

Note that a sample as thin as 10 μm may be considered 'thick' when the sample is subjected to radiation with a short penetration depth such as alpha radiation at typical source energies (see Fig. 4). The same sample, or even much thicker samples, would be considered 'thin' when subjected to beta radiation, as can be seen from Fig. 3.

5.2. Thin sample

If the ray travels completely through the sample, the theory of the previous section no longer applies and a new theory that accounts for the geometry of the sample is needed. A theory is developed below for samples that are thin compared to the radiation penetration depth and this theory is applied to samples in the shape of spheres or cylinders. For cylinders, two orientations between the cylinder and the radiation source are considered.

If the ray travels completely through the sample, the number of electron–hole pairs is given by:

$$G = \frac{1}{W}\int_0^L S_\mathrm{p}\, dx \tag{87}$$

where W is the energy per electron–hole pair, L is the path length of that particular ray in the sample, dx is an element of distance that the ray traverses, and $S_\mathrm{p} = -dT/dx$ is the sample stopping power for this type of radiation. If the penetration depth of the radiation is much larger than the sample thickness, we can assume that the loss of energy by the ray is small enough that the stopping power is approximately constant, then:

$$G = \frac{S_\mathrm{p}}{W}\, L \tag{88}$$

Consequently, for a fixed incident energy T, the value of G for some ray is proportional to the path length of that particular ray through the sample, L. It follows that for mono-energetic radiation sources:

$$\overline{G^n} = \left(\frac{S_\mathrm{p}}{W}\right)^n\, \overline{L^n} \tag{89}$$

where $\overline{L^n}$ is the statistical average of L^n over all paths of the ray through the material weighted by the probability of each path. As shown in Table 1, we know that the major statistical properties of irradiation depend on the raw moments $\overline{G^n}$. From Eq. (89), we know that $\overline{G^n}$ is proportional to $\overline{L^n}$. Consequently, to understand the statistics of different sample or grain shapes, we can focus on evaluating $\overline{L^n}$. We will calculate $\overline{L^n}$ first for a sphere and then for two orientations of a cylinder.

From the variable G column of Table 1, we see that various ratios of $\overline{G^n}$ appear of the form $\overline{G^{a\times b}}/\overline{G^a}^b$. It is useful to note that from Eq. (89) these ratios are independent of the type of radiation and solely determined by geometry:

$$\frac{\overline{G^{a\times b}}}{\overline{G^a}^b} = \frac{\overline{L^{a\times b}}}{\overline{L^a}^b} \tag{90}$$

These ratios will be tabulated for each of the geometries considered below.

These calculations are for monoenergetic radiation. If the radiation has a wide energy distribution, one would need to start with Eq. (88) and consider both S_p and L as statistical variables.

5.2.1. Sphere

We will obtain the values of $\overline{L^n}$ for a spherical sample of diameter d. The sphere has a projected area of:

$$A = \frac{\pi}{4}d^2 \tag{91}$$

If a ray travels through the sphere at an offset distance r from the center of the sphere, then the path length L of the ray through the sphere is $L = 2\sqrt{(d/2)^2 - r^2}$. We average the nth power of this path length over the sphere's projected area:

$$\overline{L^n} = \frac{\int_0^{d/2}\int_0^{2\pi} L^n r d\theta dr}{\frac{\pi}{4}d^2} \tag{92}$$

$$= \frac{\int_0^{d/2}\int_0^{2\pi}\left(2\sqrt{(d/2)^2 - r^2}\right)^n r d\theta dr}{\frac{\pi}{4}d^2} \tag{93}$$

$$= \frac{2}{n+2}d^n \tag{94}$$

Note that the product of the projected area A and the mean path length $\overline{L}$ is:

$$A\overline{L} = \left(\frac{\pi}{4}d^2\right)\left(\frac{2}{3}d\right) = \frac{\pi}{6}d^3 = V_{\text{sph}} \tag{95}$$

where V_{sph} is the volume of the sphere.

The raw moments Eq. (94), combined with Eq. (89) and the equations of Section 3.2 (Table 1), are sufficient to compute the basic statistical properties of mean, standard deviation, skewness, and kurtosis. If we want to compute the actual probability distribution of the number of trapped elections, we need f_G:

$$f_G \approx 2G/{G_{\max}}^2 \qquad \text{for } 0 \le G \le G_{\max} \tag{96}$$

where $G_{\max}$ is the value of G for a track that passes through the sphere's center:

$$G_{\max} = \frac{S_p\, d}{W} \tag{97}$$

where S_p is the stopping power and W is the energy per electron–hole pair.

5.2.2. Cylinder

For the path of a ray through a cylindrical sample, we will consider two orientations: transverse and axial. If a cylinder has diameter d and length l, then, in the transverse orientation, it has a projected area of:

$$A = dl \tag{98}$$

Table 4
Raw moment values are shown for various sample shapes and orientations. The results for spheres are from Eq. (94) while the results for cylinders are from Eq. (101) (transverse orientation) and Eq. (104) (axial orientation). The ratios provided here are the ones useful for calculating standard deviation, skewness, and kurtosis in the variable G model (see Table 1). While the values for $\overline{L^n}$ are exact, the values for the ratios have been rounded to three decimals.

Shape	$\overline{L}$	$\overline{L^2}$	$\overline{L^3}$	$\overline{L^4}$	$\overline{L^2}/\overline{L}^2$	$\overline{L^3}/\overline{L^2}^{3/2}$	$\overline{L^4}/\overline{L^2}^2$
Sphere	$\frac{2}{3}d$	$\frac{1}{2}d^2$	$\frac{2}{5}d^3$	$\frac{1}{3}d^4$	1.125	1.131	1.333
Cylinder, transverse	$\frac{\pi}{4}d$	$\frac{2}{3}d^2$	$\frac{3\pi}{16}d^3$	$\frac{8}{15}d^4$	1.081	1.082	1.200
Cylinder, axial	l	l^2	l^3	l^4	1	1	1

If a ray passes through the cylinder at an offset distance r from the axis of the cylinder, then the path length L of the ray is $L = 2\sqrt{(d/2)^2 - r^2}$. We average the nth power of this path length over the sphere's projected area:

$$\overline{L^n} = \frac{\int_0^l 2\int_0^{d/2}\left(2\sqrt{(d/2)^2 - r^2}\right)^n dr dl}{d\ l} \tag{99}$$

This reduces to:

$$\overline{L^n} = d^n \int_0^1 (1-t^2)^{n/2} dt \tag{100}$$

$$= \frac{B(\frac{1}{2}, \frac{2+n}{2})}{2}\, d^n \tag{101}$$

where $B(x, y)$ is the beta function (Gradshteyn and Ryzhik, 1965; Abramowitz and Stegun, 1970). Values for the first four raw moments are given in Table 4. Again, the product of the projected area and the mean path length is:

$$A\overline{L} = \left(d\ l\right)\left(\frac{B(\frac{1}{2}, \frac{3}{2})}{2}\, d\right) = \frac{\pi}{4}d^2 l = V_{\text{cyl}} \tag{102}$$

where V_{cyl} the cylinder volume.

To compute the trap occupation probability distribution, P_i, itself, we will also need the factors f_G: @

$$f_G = \frac{G/G_{\max}}{\sqrt{{G_{\max}}^2 - G^2}} \tag{103}$$

where again $G_{\max} = S_p d/W$.

If the ray approaches the cylinder parallel to the axis, then the path length is simply l and:

$$\overline{L^n} = l^n \tag{104}$$

Formulas for $\overline{L^n}$ and ratios of $\overline{L^n}$ for various geometries are summarized in Table 4.

6. Results

Using the master equation of Section 3, the irradiation model of Section 4, and the geometrical model of Section 5, the statistical properties of the irradiation process of thermoluminescent materials can be calculated. We will present some sample calculations for both spherical and cylindrical sample shapes. A key result is that the noise level in the irradiation process, as measured by the standard deviation of the trap population, is much larger than might be expected from a Poisson process model.

As the first example, consider a sphere of silica of diameter d = 0.00472 cm (47 μm or 0.186 mil) and irradiated by 1 MeV beta rays. From Eq. (78) or Berger et al. (2005), ICRU (1984), the stopping power of these rays in silica is 3.6×10^6 eV/cm. A 1 MeV beta ray in silica has a range of 0.2 cm and since this is much larger than the diameter d, the 'thin' sphere theory of Section 5.2 applies. From Table 3, an electron–hole pair is created in silica on average for every W = 17 eV

of energy deposited. Thus, a single beta ray passing through the center of the sphere will generate (Eq. (89)):

$$G_{\max} = \frac{S_{\mathrm{p}}}{W} d \tag{105}$$

$$= \frac{3.6\times10^{6}\ \mathrm{eV/cm}}{17\ \mathrm{eV}} \times 0.00472\ \mathrm{cm} \tag{106}$$

$$= 1000\ \text{electron–hole pairs} \tag{107}$$

This number can also be read from Fig. 3 using d as the material thickness. Even if we suppose that our silica sample is exceptionally pure, say N as low as 10^{10} cm^{-3}, we have $\mathbb{N} = VN \sim 10^5$, and the assumption $\overline{G} \ll \mathbb{N}$ is well satisfied. Thus, the large G model does not apply while, for low doses, the variable G model of Section 3.2 does.

For the average ray passing through the sphere, Eq. (89) can be combined with the formula for $\overline{L}$ (Eq. (94) or Table 4) to find:

$$\overline{G} = \frac{S_{\mathrm{p}}}{W}\ \overline{L} \tag{108}$$

$$= \frac{S_{\mathrm{p}}}{W}\left(\frac{2}{3}d\right) \tag{109}$$

$$= 667\ \text{electron–hole pairs} \tag{110}$$

This number can also be read from Fig. 3 using $\overline{L} = (2/3)d$ as the material thickness. The standard deviation in the number of electrons in the traps after irradiation is found from Eq. (50) (see Table 1):

$$\sigma = \sqrt{\left(\frac{\overline{G^2}}{\overline{G}^2}\right)\overline{G}\mathbb{E}[i]} \tag{111}$$

$$= \sqrt{1.125\times667\ \mathbb{E}[i]} \tag{112}$$

$$= \sqrt{750\ \mathbb{E}[i]} \tag{113}$$

where $\mathbb{E}[i]$ is the expected value of the trap population. The ratio $\overline{G^2}/\overline{G}^2$ was evaluated using Eq. (90) and the theory for a sphere in Section 5.2.1 as summarized in Table 4.

σ is the standard deviation of the total number of filled electron traps in the whole of the sample of volume V. The standard deviation of the trap *concentration* is:

$$\sigma_n = \frac{\sigma}{V} = \sqrt{750\ n/V} \tag{114}$$

where $n = \mathbb{E}[i]/V$ is the *expected value* of trap concentration. From Eq. (41) and for a fixed dose D, $\mathbb{E}[i] \propto V$ and, thus, by Eq. (113), σ scales with $V^{1/2}$. By contrast, from Eq. (114), the standard deviation of the trap *concentration* σ_n at fixed dose scales with $V^{-1/2}$.

The dispersion for this sample is:

$$\mathbb{D} \equiv \frac{\sigma^2}{\mathbb{E}[i]} = \frac{\overline{G^2}}{\overline{G}^2}\ \overline{G} = \frac{\overline{L^2}}{\overline{L}^2}\ \overline{G} = 1.125\times667 = 750 \tag{115}$$

This is nearly three orders of magnitude larger than the dispersion of a Poisson process.

The skewness and kurtosis of the distribution can also be computed. Continuing to consider the spherical sample and combining Eqs. (55) and (90) with Eq. (101) (see Table 4), the skewness is:

$$\widetilde{\mu_3} = \frac{\overline{G^3}}{\overline{G^2}^{3/2}}\sqrt{\frac{\overline{G}}{VD}} \tag{116}$$

$$= \frac{\overline{L^3}}{\overline{L^2}^{3/2}}\sqrt{\frac{\overline{G}}{VD}} \tag{117}$$

$$= 1.131\sqrt{\frac{667}{VD}} \tag{118}$$

$$= \sqrt{\frac{853}{VD}} \tag{119}$$

Similarly, for kurtosis:

$$\widetilde{\mu_4} = 3 + \frac{\overline{G^4}}{\overline{G^2}^2}\frac{\overline{G}}{VD} \tag{120}$$

$$= 3 + \frac{\overline{L^4}}{\overline{L^2}^2}\frac{\overline{G}}{VD} \tag{121}$$

$$= 3 + 1.333\ \frac{667}{VD} \tag{122}$$

$$= 3 + \frac{889}{VD} \tag{123}$$

For a normal (Gaussian) distribution, $\widetilde{\mu_3} = 0$ and $\widetilde{\mu_4} = 3$. Eqs. (119) and (123) show that, initially, when dose or $\mathbb{E}[i]$ is close to zero, the distribution has large skewness and kurtosis. As dose increases, the distribution approaches Gaussian.

The above results were obtained analytically. To find the actual probability distribution, P_i, we will solve the master equation Eq. (30)

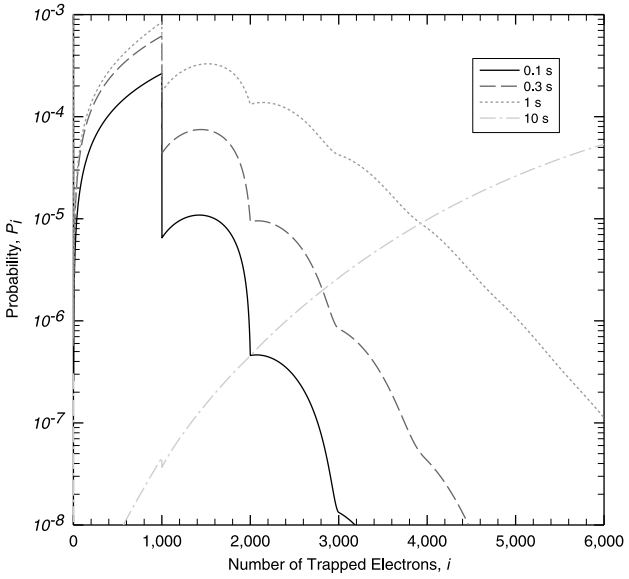

Fig. 5. A sample calculation was performed for the probability distribution of trap population, P_i, in a spherical sample during irradiation. Probabilities P_i are plotted against the number of occupied traps, i, for four different exposure times. The sample was assumed to be spherical, made of silica, and having a stopping power sufficient to generate 1000 electrons in a radiation track passing through the diameter.

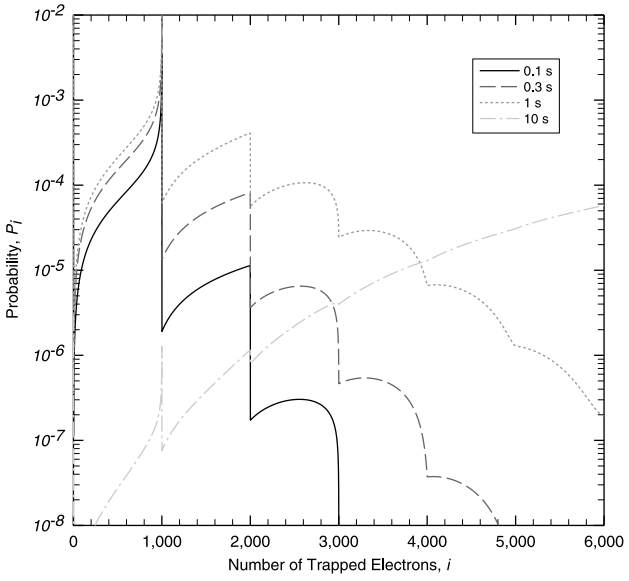

Fig. 6. The probability distribution of trap population, P_i, is plotted against the number of occupied traps, i, for a cylindrical silica sample exposed to beta irradiation. Other than shape, the same parameters as in Fig. 5 are used.

numerically. We will continue considering the $d = 0.00472$ cm silica sphere irradiated by 1 MeV beta rays. P_i is the probability that i traps are filled and it varies as a function of time t as determined by Eq. (30). Results for P_i, starting from initially empty traps (Eq. (20)), are shown in Fig. 5 for an irradiation rate of $X = 1.16{\times}10^8$ cm^3/s. At time $t = 0.1$ s, most of the traps are still empty. Among the non-empty traps, there is a local peak of probability at $i = 1000$ trapped electrons. There is also smaller peak at $i = 1423$. As time goes on, the distribution broadens out. By $t = 10$ s, the distribution begins to resemble a Gaussian distribution.

A striking feature of Fig. 5 is sharp drop in probability that is seen at 1000 trapped electrons. This is because the diameter of the sphere was chosen so that one ray passing through the diameter creates 1000 ionizations. In other words, $G_{\max} = 1000$. This means that any random ray passing through may create from 0 to 1000 ionizations but never 1001 or more. Thus, a single ray can create 1000 ionizations but 1001 ionizations requires two or more rays. This is why, when starting from empty traps and at the lowest doses, you see a peak at 1000 and discontinuous drop between 1000 and 1001. This effect continues, but weakens, at multiples of $G_{\max}$. For example, a concentration of 2000 can be achieved with just two rays but 2001 requires at least three.

For comparison, consider a cylindrical sample of silica of the same diameter and volume as the spherical sample considered above and oriented with its axis *transverse* to the incoming radiation. Because this cylinder has the same diameter as the sphere, the value of $G_{\max}$ remains the same:

$$G_{\max} = \frac{S_{\mathrm{p}}}{W} d \tag{124}$$

$$= \frac{3.6{\times}10^5 \text{ eV/cm}}{17 \text{ eV}} \times 0.00472 \text{ cm} \tag{125}$$

$$= 1000 \text{ electron–hole pairs} \tag{126}$$

Because of the cylindrical shape, however, the value of $\overline{G}$ is different:

$$\overline{G} = \frac{S_{\mathrm{p}}}{W} \overline{L} \tag{127}$$

$$= \frac{S_{\mathrm{p}}}{W} \left(\frac{\pi}{4} d\right) \tag{128}$$

$$= 785 \text{ electron–hole pairs} \tag{129}$$

where the value of $\overline{L}$ was evaluated from Eq. (101) (see also Table 4). This number can also be read from Fig. 3 using $\overline{L} = (\pi/4)d$ as the material thickness. The standard deviation in the number of electrons in the traps after irradiation is found from Eq. (50) (see Table 1):

$$\sigma = \sqrt{\left(\frac{\overline{G^2}}{\overline{G}^2}\right) \overline{G} \mathbb{E}[i]} \tag{130}$$

$$= \sqrt{\left(\frac{\overline{L^2}}{\overline{L}^2}\right) \overline{G} \mathbb{E}[i]} \tag{131}$$

$$= \sqrt{1.081 \times 785 \ \mathbb{E}[i]} \tag{132}$$

$$= \sqrt{848 \ \mathbb{E}[i]} \tag{133}$$

where the ratio $\overline{G}^2/\overline{G}^2$ was evaluated using Eq. (90) and the theory for a cylinder in transverse orientation in Section 5.2.2 as summarized in Table 4. The dispersion for this sample is:

$$\mathbb{D} \equiv \frac{\sigma^2}{\mathbb{E}[i]} = 848 \tag{134}$$

Again, this is three orders of magnitude larger than the dispersion of a Poisson process.

The probability distribution P_i for trap population i for this cylindrical silica sample after irradiation can be calculated numerically and is shown in Fig. 6. For the cylinder, the peaks in the distribution at $i = G_{\max} = 1000$ are much taller and sharper than for the sphere. This is because the shape of f_G differs greatly between a sphere, Eq. (96), and a cylinder, Eq. (103). The $i = G_{\max} = 1000$ peak is strong even at $t = 10$ s where the distribution has otherwise developed into a nearly Gaussian shape.

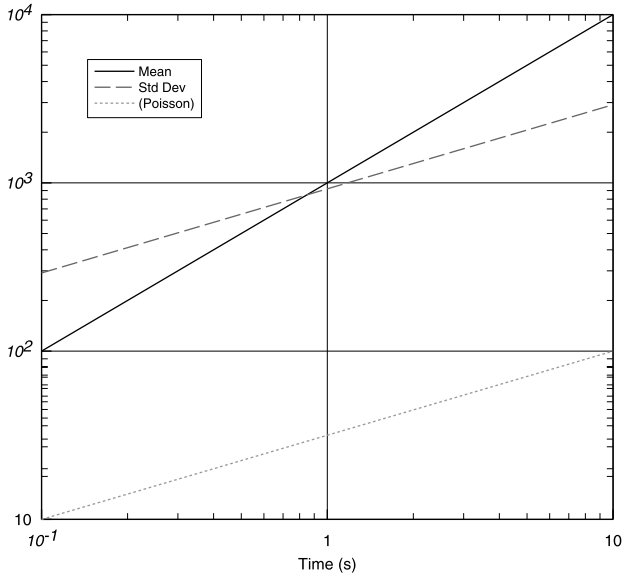

Fig. 7. The mean $\mathbb{E}[i]$ (solid) and standard deviation σ (dashed) of the population of occupied traps corresponding to Fig. 6 are plotted against irradiation time. For comparison, the much smaller standard deviation σ (dotted) of a Poisson distribution with the same mean is also shown.

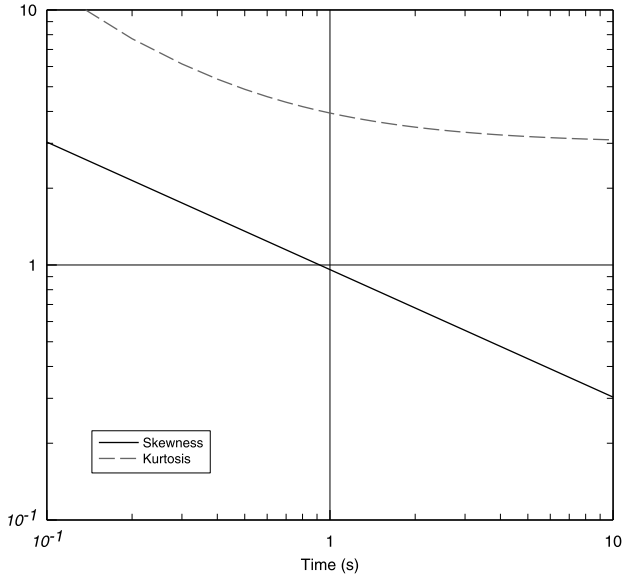

Fig. 8. The skewness and kurtosis of the probability distribution of occupied traps are plotted against time under the same assumptions as used for Fig. 6. The large kurtosis for short irradiation times means that experiments will see more-than-expected outliers while the large skewness means more of those outliers will be at the high side than the low side.

Even when the distribution achieves a Gaussian distribution, the standard deviation is large. The mean and standard deviation for the cylindrical case are shown in Fig. 7. For comparison, the plot also shows the standard deviation of a Poisson process with the same mean. The actual standard deviation for this process is over an order of magnitude larger than what it would be for a Poisson process. Fig. 7 shows mean and standard deviation increasing as dose increases. Both continue to increase with increasing dose as long as the dose is below saturation (as defined by Eqs. (12) and (29)). As the dose

approaches saturation, the mean would approach a limit while the standard deviation returns to zero.

Fig. 8 shows the skewness and kurtosis of the probability distribution for the cylindrical sample in Fig. 6. The combination of large positive skewness and large kurtosis means that experimental results would have 'outliers' on the large signal side.

The distributions in Figs. 5 and 6 are the result of numerical integration of Eq. (30) using the `scipy.integrate.odeint` solver under Python version 3.7. The numerical method solved 30,000 simultaneous differential equations for trap occupation numbers $0 \le i < 30{,}000$. Calculation time was less than two minutes.

Finally, the importance of orientation can be illustrated by considering a larger longer cylinder, $d = 0.1$ mm in diameter and $\ell = 1$ mm long, made of alumina and subjected to 2 MeV beta rays. At 2 MeV, the stopping power is about 3.6 MeV/cm and the range is about 5 mm, again justifying the use of the thin sample model. As before, for the case of irradiation coming *transverse* to the cylinder axis, we can calculate the standard deviation for the number of trapped electrons after irradiation as:

$$\sigma = \sqrt{\left(\frac{\overline{G^2}}{\overline{G}^2}\right)\overline{G}\,\mathbb{E}[i]} \tag{135}$$

$$= \sqrt{\left(\frac{\overline{L^2}}{\overline{L}^2}\right)\frac{S_P}{W}\left(\frac{\pi}{4}\right)d\,\mathbb{E}[i]} \tag{136}$$

$$= \sqrt{1.081 \times 1660\ \mathbb{E}[i]} \tag{137}$$

$$= \sqrt{1800\ \mathbb{E}[i]} \qquad \text{for the transverse orientation} \tag{138}$$

By contrast, if the radiation arrives along the *axial* direction, the standard deviation of trapped electrons is:

$$\sigma = \sqrt{\left(\frac{\overline{G^2}}{\overline{G}^2}\right)\,\overline{G}\,\mathbb{E}[i]} \tag{139}$$

$$= \sqrt{\left(\frac{\overline{L^2}}{\overline{L}^2}\right)\left(\frac{S_P}{W}\,\ell\right)\mathbb{E}[i]} \tag{140}$$

$$= \sqrt{1 \times 21{,}200\ \mathbb{E}[i]} \tag{141}$$

$$= \sqrt{21{,}200\ \mathbb{E}[i]} \qquad \text{for the axial orientation} \tag{142}$$

For a cylinder with these dimensions, while the dispersion is 1800 when the radiation is *transverse*, it is an order of magnitude larger, 21,200, when the radiation is along the *axial* direction. In other words, even if one is using the same sample material in a thermoluminescence measurement, the statistics of the glow curve can vary depending on the orientation of the sample to the radiation source.

7. Summary and conclusions

The present work divides into two parts. The first part developed a general model for the statistical behavior of irradiation of a one-trap one-center system at low dose. It found that the statistical properties, such as standard deviation and skewness, can be determined from raw moments, $\overline{G^n}$, of the number of electron–hole pairs created by each radiation track. The second part developed a simplified model for alpha or beta radiation that enable estimates of the raw moments $\overline{G^n}$ to be made for various particle energies and sample geometries. Some key points are:

- The irradiation process of a thermoluminescent material is statistical and, if the same experiment is performed multiple times, different numbers of trapped electrons will be created. The average number of trapped electrons is predicted by the conventional phenomenological theory. The theory developed herein predicts the standard deviation and other statistical features of the number of trapped electrons after irradiation.
- This study is motivated by the large standard deviations observed in single-grain experiments. Note that we have not addressed any instrumental sources of noise. This theory is focused on the noise and statistics inherent to the physical process of irradiation.
- For alpha, beta, or gamma irradiation, the predicted standard deviation and dispersion can be orders of magnitude larger than one might expect from a conventional Poisson process model.
- The statistics of the irradiation process depend not just on the thermoluminescent material and type of radiation but also on the size, shape, and orientation of the material. We examined a sample case where the dispersion varied by an order of magnitude when merely the orientation of sample was changed.
- At low doses or under some other conditions, experimental data may show more outliers than would be expected for data with a Gaussian distribution. This is quantified by the calculations of skewness and kurtosis herein. For these conditions, the statistical analyzes that assume a Gaussian distribution should not be used to assess the data.

The simplified model of irradiation enables, in many cases, simple analytical formulas for the statistical properties of irradiation. In cases where more accuracy is desired or in more complex cases, where, for example, there might be backscattered radiation from the sample holder (Hansen et al., 2018; Kumar, 2019; Tabata and Ito, 1992) or the sample might be small enough that secondary electrons escape or particle energy might be low enough that the straight-track approximation is not useful, more sophisticated numerical models of radiation transport would be needed (Kawrakow, 2000; Sood, 2017; Salvat et al., 2007; Nuclear Energy Agency, 2019; Nikjoo et al., 2006; Agostinelli et al., 2003; Allison et al., 2006). Such a radiation transport model would replace simplified models in Sections 4 and 5 but the model of Section 3 would remain valid and could be used to analyze the results.

Declaration of competing interest

The authors declare that they have no known competing financial interests or personal relationships that could have appeared to influence the work reported in this paper.

Appendix A. Moments of fixed-G distribution

To compute the statistical properties of the fixed-G model, we will start by taking raw k-moments of the distribution:

$$\mu'_k = \sum_{i=0}^{\infty} i^k P_i \tag{A.1}$$

where P_i is given by the fixed-G distribution in Eq. (21). Note that P_i in Eq. (21) is zero unless i is an integer multiple of G_*. Keeping only the non-zero terms, we have:

$$\mu'_k = \sum_{j=0}^{\infty} (jG_*)^k P_{jG_*} \tag{A.2}$$

$$= {G_*}^k \left[\sum_{j=0}^{\infty} j^k \frac{(VD/G_*)^j}{j!} e^{-VD/G_*}\right] \tag{A.3}$$

The quantity in square brackets in Eq. (A.3) is simply the kth raw moment of the standard Poisson distribution of parameter VD/G_*. As these are well-known, we can immediately write:

$$\mu'_0 = 1 \tag{A.4}$$

$$\mu'_1 = G_*\,(VD/G_*) \tag{A.5}$$

$$\mu'_2 = {G_*}^2\left[(VD/G_*)^2 + (VD/G_*)\right] \tag{A.6}$$

$$\mu'_3 = {G_*}^3\left[(VD/G_*)^3 + 3(VD/G_*)^2 + (VD/G_*)\right] \tag{A.7}$$

$$\mu'_4 = {G_*}^4\left[(VD/G_*)^4 + 6(VD/G_*)^3 + 7(VD/G_*)^2 + (VD/G_*)\right] \tag{A.8}$$

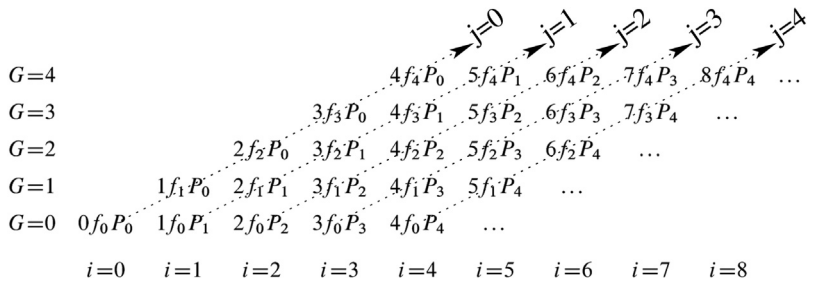

Fig. C.9. The terms in the summation of Eq. (C.1) are shown. In Eq. (C.1), the inner sum is over G and the outer sum is over i. The inner sum is limited to $0 \le G \le i$. In Eq. (C.6), by contrast, we introduce j which labels diagonals with the inner sum being over j and the outer sum being over G. The same terms are summed in both Eqs. (C.1) and (C.6), only the order in which they are summed has changed.

It follows from the definitions that the mean, standard deviation, skewness, and kurtosis of the fixed-G distribution are given by:

$$\mathbb{E}[i] = \mu_1' = VD \tag{A.9}$$

$$\sigma = \sqrt{\mu_2' - \mu_1'^2} = G_* VD \tag{A.10}$$

$$\widetilde{\mu_3} = \sqrt{\frac{\mu_3' - 3\mu_2'\mu_1' + 2\mu_1'^3}{\left(\mu_2' - \mu_1'^2\right)^{3/2}}} = \sqrt{\frac{G_*}{VD}} \tag{A.11}$$

$$\widetilde{\mu_4} = \frac{\left(\mu_4' - 4\mu_3'\mu_1' + 6\mu_2'\mu_1'^2 - 3\mu_1'^4\right)}{\sigma^2} = 3 + \frac{G_*}{VD} \tag{A.12}$$

These results for fixed-G are summarized and compared to the other models in Table 1.

Appendix B. Calculation of μ_k

We do not have a general *analytical* solution for the trap occupancy distribution for the variable-G case. We can, subject to the low-dose approximation, obtain general information about the central *moments* of the distribution as defined by:

$$\mu_k = \sum_{i\ge 0} \left(i - \mathbb{E}[i]\right)^k P_i \tag{B.1}$$

where k is an integer and μ_k is a central moment. Differentiating Eq. (B.1):

$$\frac{d\mu_k}{dt} = \sum_{i\ge 0} \left(i - \mathbb{E}[i]\right)^k \frac{dP_i}{dt} - k \sum_{i\ge 0} \left(i - \mathbb{E}[i]\right)^{k-1} P_i \frac{d\mathbb{E}[i]}{dt} \tag{B.2}$$

$$= \sum_{i\ge 0} \left(i - \mathbb{E}[i]\right)^k \frac{dP_i}{dt} - k\ \mu_{k-1}\ \mathbb{X}\overline{G} \tag{B.3}$$

where Eqs. (37), (17), and (B.1) were used. Evaluating $\frac{dP_i}{dt}$ using the master Eqs. (30), (B.3) can be further reduced:

$$\frac{d\mu_k}{dt} = \mathbb{X} \sum_{i\ge 0} \sum_{G=0}^{i} f_G \left(i - \mathbb{E}[i]\right)^k P_{i-G} - \mathbb{X} \sum_{i\ge 0} \sum_{G\ge 0} f_G \left(i - \mathbb{E}[i]\right)^k P_i - k\ \mu_{k-1}\ \mathbb{X}\overline{G} \tag{B.4}$$

$$= \mathbb{X} \sum_{j\ge 0} \sum_{G\ge 0} f_G \left(j + G - \mathbb{E}[i]\right)^k P_j - \mathbb{X}\left(\sum_{G\ge 0} f_G\right)\left(\sum_{i\ge 0} \left(i - \mathbb{E}[i]\right)^k P_i\right) - k\ \mu_{k-1}\ \mathbb{X}\overline{G} \tag{B.5}$$

$$= \mathbb{X} \sum_{j\ge 0} \sum_{G\ge 0} \sum_{\ell=0}^{k} \binom{k}{\ell} f_G G^l \left(j - \mathbb{E}[i]\right)^{k-l} P_j - \mathbb{X}\mu_k - k\ \mu_{k-1}\ \mathbb{X}\overline{G} \tag{B.6}$$

$$= \mathbb{X} \sum_{\ell=0}^{k} \binom{k}{\ell} \left(\sum_{G\ge 0} f_G G^\ell\right)\left(\sum_{j\ge 0} \left(j - \mathbb{E}[i]\right)^{k-\ell} P_j\right) - \mathbb{X}\mu_k - k\ \mu_{k-1}\ \mathbb{X}\overline{G} \tag{B.7}$$

$$= \mathbb{X} \sum_{\ell=0}^{k} \binom{k}{\ell} \overline{G^\ell}\, \mu_{k-\ell} - \mathbb{X}\mu_k - k\ \mathbb{X}\overline{G}\mu_{k-1} \tag{B.8}$$

$$= \mathbb{X} \sum_{\ell=2}^{k} \binom{k}{\ell} \overline{G^\ell}\, \mu_{k-\ell} \tag{B.9}$$

where $\binom{k}{\ell}$ is the binomial coefficient:

$$\binom{k}{\ell} = \frac{k!}{(k-\ell)!\ \ell!} \tag{B.10}$$

and $\overline{G^\ell}$ is defined by Eq. (47). Let us summarize the behavior of the first five central moments of μ_k. From the definition of μ_k, Eq. (B.1), we have trivially:

$$\mu_0 = 1 \tag{B.11}$$

$$\mu_1 = 0 \tag{B.12}$$

For the next three central moments, we do not know their values but Eq. (B.9) does give us their time derivatives:

$$\frac{d\mu_2}{dt} = \mathbb{X}\overline{G^2} \tag{B.13}$$

$$\frac{d\mu_3}{dt} = \mathbb{X}\overline{G^3} \tag{B.14}$$

$$\frac{d\mu_4}{dt} = \mathbb{X}\left(6\overline{G^2}\mu_2 + \overline{G^4}\right) \tag{B.15}$$

Eq. (B.13) through Eq. (B.15) are used to compute the standard deviation, skewness, and kurtosis under the large-G model of Section 3.3.

Appendix C. Reversing order of summation

To proceed from Eq. (33) to Eq. (34), we need to reverse the order of summation of the first term on the right-hand-side of Eq. (33). The sum in question is:

$$\text{Sum} = \sum_{i\ge 0} \sum_{G=0}^{i} f_G i P_{i-G} \tag{C.1}$$

Because the inner sum has an upper limit, i, that is dependent on the outer sum, reversing the order of the sums requires care.

We introduce a delta function defined by:

$$\delta_{G\le i} \equiv \begin{cases} 1 & \text{for } G \le i \\ 0 & \text{for } G > i \end{cases} \tag{C.2}$$

Using Eq. (C.2), we can rewrite Eq. (C.1):

$$\text{Sum} = \sum_{i\ge 0} \sum_{G\ge 0} \delta_{G\le i} f_G i P_{i-G} \tag{C.3}$$

In Eq. (C.3), the limits of the two sums are now independent and, since the sum is absolutely convergent, we can interchange the order of summation:

$$\text{Sum} = \sum_{G\ge 0} \sum_{i\ge 0} \delta_{G\le i} f_G i P_{i-G} \tag{C.4}$$

Since we do not need to sum over terms that are zero, Eq. (C.4) reduces to:

$$\text{Sum} = \sum_{G\geq 0}\sum_{i\geq G} f_G i P_{i-G} \tag{C.5}$$

Now, let us introduce a new variable $j = i - G$. With this, Eq. (C.5) becomes:

$$\text{Sum} = \sum_{G\geq 0}\sum_{j\geq 0} f_G(j+G) P_j \tag{C.6}$$

The change from Eq. (C.1) to Eq. (C.6) can be illustrated as shown in Fig. C.9.

At this point, 'j' in Eq. (C.6) is just a variable of summation and we can replace it with 'i':

$$\text{Sum} = \sum_{G\geq 0}\sum_{i\geq 0} f_G(i+G) P_i \tag{C.7}$$

This is the form of the sum used in Eq. (34)

References

Abramowitz, M., Stegun, I. A. (Eds.), 1970. Handbook of Mathematical Functions. U.S. Government Printing Office, Washington, D. C.

Agostinelli, S., Allison, J., Amako, K., Apostolakis, J., Araujo, H., Arce, P., Asai, M., Axen, D., Banerjee, S., Barrand, G., Behner, F., Bellagamba, L., Boudreau, J., Broglia, L., Brunengo, A., Burkhardt, H., Chauvie, S., Chuma, J., Chytracek, R., Cooperman, G., Cosmo, G., Degtyarenko, P., Dell'Acqua, A., Depaola, G., Dietrich, D., Enami, R., Feliciello, A., Ferguson, C., Fesefeldt, H., Folger, G., Foppiano, F., Forti, A., Garelli, S., Giani, S., Giannitrapani, R., Gibin, D., Gómez Cadenas, J.J., González, I., Abril, G.Gracia., Greeniaus, G., Greiner, W., Grichine, V., Grossheim, A., Guatelli, S., Gumplinger, P., Hamatsu, R., Hashimoto, K., Hasui, H., Heikkinen, A., Howard, A., Ivanchenko, V., Johnson, A., Jones, F.W., Kallenbach, J., Kanaya, N., Kawabata, M., Kawabata, Y., Kawaguti, M., Kelner, S., Kent, P., Kimura, A., Kodama, T., Kokoulin, R., Kossov, M., Kurashige, H., Lamanna, E., Lampén, T., Lara, V., Lefebure, V., Lei, F., Liendl, M., Lockman, W., Longo, F., Magni, S., Maire, M., Medernach, E., Minamimoto, K., Freitas, P.Mora.de., Morita, Y., Murakami, K., Nagamatu, M., Nartallo, R., Nieminen, P., Nishimura, T., Ohtsubo, K., Okamura, M., O'Neale, S., Oohata, Y., Paech, K., Perl, J., Pfeiffer, A., Pia, M.G., Ranjard, F., Rybin, A., Sadilov, S., Salvo, E.Di., Santin, G., Sasaki, T., Savvas, N., Sawada, Y., Scherer, S., Sei, S., Sirotenko, V., Smith, D., Starkov, N., Stoecker, H., Sulkimo, J., Takahata, M., Tanaka, S., Tcherniaev, E., Tehrani, E.Safai., Tropeano, M., Truscott, P., Uno, H., Urban, L., Urban, P., Verderi, M., Walkden, A., Wander, W., Weber, H., Wellisch, J.P., Wenaus, T., Williams, D.C., Wright, D., Yamada, T., Yoshida, H., Zschiesche, D., 2003. Geant4—a simulation toolkit. Nucl. Instrum. Methods Phys. Res. A 506 (3), 250–303, URL https://www.sciencedirect.com/science/article/pii/S0168900203013688.

Aitken, M.J., 1985. Thermoluminescence Dating. Academic Press, London.

Alig, R.C., Bloom, S., 1975. Electron–hole-pair creation energies in semiconductors. Phys. Rev. Lett. 35, 1522–1525, URL https://link.aps.org/doi/10.1103/PhysRevLett.35.1522.

Allison, J., Amako, K., Apostolakis, J., Araujo, H., Dubois, P.A., Asai, M., Barrand, G., Capra, R., Chauvie, S., Chytracek, R., Cirrone, G.A.P., Cooperman, G., Cosmo, G., Cuttone, G., Daquino, G.G., Donszelmann, M., Dressel, M., Folger, G., Foppiano, F., Generowicz, J., Grichine, V., Guatelli, S., Gumplinger, P., Heikkinen, A., Hrivnacova, I., Howard, A., Incerti, S., Ivanchenko, V., Johnson, T., Jones, F., Koi, T., Kokoulin, R., Kossov, M., Kurashige, H., Lara, V., Larsson, S., Lei, F., Link, O., Longo, F., Maire, M., Mantero, A., Mascialino, B., McLaren, I., Lorenzo, P.M., Minamimoto, K., Murakami, K., Nieminen, P., Pandola, L., Parlati, S., Peralta, L., Perl, J., Pfeiffer, A., Pia, M.G., Ribon, A., Rodrigues, P., Russo, G., Sadilov, S., Santin, G., Sasaki, T., Smith, D., Starkov, N., Tanaka, S., Tcherniaev, E., Tome, B., Trindade, A., Truscott, P., Urban, L., Verderi, M., Walkden, A., Wellisch, J.P., Williams, D.C., Wright, D., Yoshida, H., 2006. Geant4 developments and applications. IEEE Trans. Nucl. Sci. 53 (1), 270–278. http://dx.doi.org/10.1109/TNS.2006.869826.

Arshak, K., Korostynska, O., 2006. Advanced Materials and Techniques for Radiation Dosimetry. Artech House, Boston.

Attix, F.H., 2004. Introduction to Radiological Physics and Radiation Dosimetry. John Wiley and Sons.

Barnett, A.M., Lees, J.E., Bassford, D.J., 2013. Temperature dependence of the average electron–hole pair creation energy in $al_{0.8}ga_{0.2}as$. Appl. Phys. Lett. 102 (18), 181119. http://dx.doi.org/10.1063/1.4804989.

Berger, M.J., Coursey, J.S., Zucker, M.A., Chang, J., 2005. ESTAR, PSTAR, and ASTAR: Computer Programs for Calculating Stopping-Power and Range Tables for Electrons, Protons, and Helium Ions (Version 1.2.3). [Online]. Tech. Rep., National Institute of Standards and Technology, Gaithersburg, MD, URL http://physics.nist.gov/Star.

Bøtter-Jensen, L., Bulur, E., Duller, G.A.T., Murray, A., 2000. Advances in luminescence instrumentation. Radiat. Meas. 32, 523–528.

Bräunlich, P., 1990. Present state and future of TLD laser heating. Radiat. Prot. Dosim. 34, 345–351.

Chen, R., McKeever, S.W.S., 1997. Theory of Thermoluminescence and Related Phenomena. World Scientific, London.

Chen, R., Pagonis, V., 2011. Thermally and Optically Stimulated Luminescence: A Simulation Approach. John Wiley & Sons, Ltd.

Dalgarno, A., 1962. Range and energy loss. In: Bates, D.R. (Ed.), Atomic and Molecular Processes. p. 623.

Dendy, R.O., 1990. Plasma Dynamics. Oxford Science Publications. Clarendon Press, URL https://books.google.com/books?id=rCm3QgAACAAJ.

Duller, G.A.T., 2004. Luminescence dating of quaternary sediments: recent advances. J. Quatern. Sci. 19 (2), 183–192, URL https://onlinelibrary.wiley.com/doi/abs/10.1002/jqs.809.

Duller, G.A.T., Bøtter-Jensen, L., Murray, A.S., Truscott, A.J., 1999. Single grain laser luminescence (SGLL) measurements using a novel automated reader. Nucl. Instrum. Methods Phys. Res. B 155 (4), 506–514, URL https://www.sciencedirect.com/science/article/pii/S0168583X99004887.

Fain, B., 1981. Theory of rate constants: Master equation approach. J. Stat. Phys. 25 (3), 475.

Fernández-Varea, J., Andreo, P., Tabata, T., 1996. Detour factors in water and plastic phantoms and their use for range and depth scaling in electron-beam dosimetry. Phys. Med. Biol. 41, 1119–1139.

Fokker, A.D., 1914. Die mittlere energie rotierender elektrischer dipole im strahlungsfeld. Ann. Phys. 348 (5), 810–820, URL https://onlinelibrary.wiley.com/doi/abs/10.1002/andp.19143480507.

Garlick, G.F.J., Gibson, A.F., 1948. The electron trap mechanism of luminescence in sulphide and silicate phosphors. Proc. R. Soc. Lond. A 60, 574–590.

Gasiot, J., Bräunlich, P., Fillard, J.P., 1982. Laser heating in thermoluminescence dosimetry. J. Appl. Phys. 53 (7), 5200–5209.

Goldstein, B., 1965. Electron–hole pair creation in gallium phosphide by α particles. J. Appl. Phys. 36 (12), 3853–3856. http://dx.doi.org/10.1063/1.1713961.

Gradshteyn, I.S., Ryzhik, I.M., 1965. Table of Integrals, Series, and Products. Academic Press, New York.

Guérin, G., Jain, M., Thomsen, K.J., Murray, A.S., Mercier, N., 2015. Modelling dose rate to single grains of quartz in well-sorted sand samples: The dispersion arising from the presence of potassium feldspars and implications for single grain OSL dating. Quatern. Geochronol. 27, 52–65, URL https://www.sciencedirect.com/science/article/pii/S1871101414001162.

Hansen, V., Murray, A., Thomsen, K., Jain, M., Autzen, M., Buylaert, J.-P., 2018. Towards the origins of over-dispersion in beta source calibration. Radiat. Meas. 120, 157–162, URL https://www.sciencedirect.com/science/article/pii/S1350448717308582 15th International Conference on Luminescence and Electron Spin Resonance Dating, 11-15 2017.

Highland, V.L., 1975. Some practical remarks on multiple scattering. Nucl. Instrum. Methods 129 (2), 497–499, URL https://www.sciencedirect.com/science/article/pii/0029554X75907430.

Highland, V.L., 1979. Erratum. Nucl. Instrum. Methods 161 (1), 171, URL https://www.sciencedirect.com/science/article/pii/0029554X79903793.

ICRU, 1984. Stopping Powers for Electrons and Positrons. Tech. Rep. 37, International Commission on Radiation Units and Measurements, Bethesda, MD, USA.

ICRU, 1993. Stopping Powers and Ranges for Protons and Alpha Particles. Tech. Rep. 49, International Commission on Radiation Units and Measurements, Bethesda, MD, USA.

Jacobs, Z., Duller, G.A.T., Wintle, A.G., 2006. Interpretation of single grain D_e distributions and calculation of D_e. Radiat. Meas. 41 (3), 264–277, URL http://www.sciencedirect.com/science/article/pii/S1350448705002404.

Jacobs, Z., Roberts, R.G., 2007. Advances in optically stimulated luminescence dating of individual grains of quartz from archeological deposits. Evol. Anthropol.: Issues News Rev. 16 (6), 210–223, URL https://onlinelibrary.wiley.com/doi/abs/10.1002/evan.20150.

Kawrakow, I., 2000. Accurate condensed history Monte Carlo simulation of electron transport. I. Egsnrc, the new EGS4 version. Med. Phys. 27 (3), 485–498, URL https://aapm.onlinelibrary.wiley.com/doi/abs/10.1118/1.598917.

Klein, C.A., 1968. Bandgap dependence and related features of radiation ionization energies in semiconductors. J. Appl. Phys. 39 (4), 2029–2038. http://dx.doi.org/10.1063/1.1656484.

Kolobov, V., 2003. Fokker—Planck modeling of electron kinetics in plasmas and semiconductors. Comput. Mater. Sci. 28, 302–320.

Kumar, M., 2019. Further considerations on towards the origins of over-dispersion in beta source calibration by hansen et al., radiation measurements, 2018. Radiat. Meas. 126, 106137, URL https://www.sciencedirect.com/science/article/pii/S1350448718305389.

Lawless, J.L., Chen, R., Pagonis, V., 2020. Inherent statistics of glow curves from small samples and single grains. J. Lumin. 226, 117389, URL https://www.sciencedirect.com/science/article/pii/S0022231320304506.

Lawless, J., Lam, S., Lo, D., 2002. Nondestructive in situ thermoluminescence using CO_2 laser heating. Opt. Express 10, 291–296.

Lax, M., 1960. Cascade capture of electrons in solids. Phys. Rev. 119 (5), 1502–1523.

Ljungberg, M., Sjögreen Gleisner, K., 2018. 3-d image-based dosimetry in radionuclide therapy. IEEE Trans. Radiat. Plasma Med. Sci. 2 (6), 527–540.

Lynch, G.R., Dahl, O.I., 1991. Approximations to multiple Coulomb scattering. Nucl. Instrum. Methods Phys. Res. B 58 (1), 6–10, URL https://www.sciencedirect.com/science/article/pii/0168583X9195671Y.

McKeever, S.W.S., 1985. Thermoluminescence of Solids. Cambridge University Press, Cambridge.

National Academy of Sciences, 1964. Studies in Penetration of Charged Particles in Matter. The National Academies Press, Washington, DC, URL https://www.nap.edu/catalog/20066/studies-in-penetration-of-charged-particles-in-matter.

Nikjoo, H., Uehara, S., Emfietzoglou, D., Cucinotta, F.A., 2006. Track-structure codes in radiation research. Radiat. Meas. 41 (9–10), 1052–1074.

Nuclear Energy Agency, 2019. PENELOPE 2018: A code system for Monte Carlo simulation of electron and photon transport. Workshop Proceedings, Barcelona, Spain, 28 January - 1 2019. post=URL https://www.oecd-ilibrary.org/content/publication/32da5043-en.

Planck, M., 1917. Über einen satz der statistischen dynamik und seine erweiterung in der quantentheorie. Sitzungsber. Preuss. Akad. Wiss. 24, 324–341.

Randall, E.A., Wilkins, M.H.F., 1945a. Phosphorescence and electron traps i. Proc. R. Soc. Lond. Ser. A 184, 366–389.

Randall, E.A., Wilkins, M.H.F., 1945b. Phosphorescence and electron traps II. Proc. R. Soc. Lond. Ser. A 184, 390–407.

Rich, .J.W., Treanor, .C.E., 1970. Vibrational relaxation in gas-dynamic flows. Annu. Rev. Fluid Mech. 2, 355–396.

Rose, A., 1955. Recombination processes in insulators and semiconductors. Phys. Rev. 97, 322–333.

Ryan, R.D., 1973. Precision measurements of the ionization energy and its temperature variation in high purity silicon radiation detectors. IEEE Trans. Nucl. Sci. 20 (1), 473–480.

Salvat, F., Fernández-Varea, J., Sempau, J., 2007. Penelope. a code system for Monte Carlo simulation of electron and photon transport. In: NEA Data Bank, Workshop Proceeding, Barcelona, pp. 4–7.

Scholze, F., Rabus, H., Ulm, G., 1998. Mean energy required to produce an electron–hole pair in silicon for photons of energies between 50 and 1500 ev. J. Appl. Phys. 84 (5), 2926–2939. http://dx.doi.org/10.1063/1.368398.

Scott, W.T., 1963. The theory of small-angle multiple scattering of fast charged particles. Rev. Modern Phys. 35, 231–313, URL https://link.aps.org/doi/10.1103/RevModPhys.35.231.

Sood, A., 2017. The Monte Carlo method and MCNP — a brief review of our 40 year history. In: Int. Topical Meeting on Industrial Radiation and Radioisotope Measurement - Applications Conference la-UR-17-26533. Los Alamos National Laboratory, Chicago, IL, URL https://laws.lanl.gov/vhosts/mcnp.lanl.gov/pdf_files/la-ur-17-26533.pdf.

Swandic, J.R., 1992. Stochastic approach to recombination luminescence with retrapping in the steady state. Phys. Rev. B 45, 622–634.

Swandic, J.R., 1996. Stochastic analysis of multiple-level recombination luminescence and retrapping in the steady state. Phys. Rev. B 53, 2352–2366.

Tabata, T., Ito, R., 1992. Simple calculation of the electron-backscatter factor. Med. Phys. 19, 1423–1426.

Turner, J.E., 2007. Atoms, Radiation, and Radiation Protection. John Wiley & Sons, Ltd., URL https://www.onlinelibrary.wiley.com/doi/abs/10.1002/9783527616978.

van Kampen, N.G., 1992. Stochastic Processes in Physics and Chemistry. Elsevier Science, Amsterdam.

Wilson, J.W., Chang, C.K., Xu, Y.J., Kamaratos, E., 1982. Ionic bond effects on the mean excitation energy for stopping power. J. Appl. Phys. 53 (2), 828–830.

Yukihara, E., McKeever, S.W.S., 2011. Optically Stimulated Luminescence: Fundamentals and Applications. John Wiley Sons Ltd.